Synchronization and Cell-Search Technique Using Preamble for OFDM Cellular Systems

Kwang Soon Kim, *Senior Member, IEEE*, Sung Woong Kim, *Student Member, IEEE*, Yong Soo Cho, *Senior Member, IEEE*, and Jae Young Ahn, *Member, IEEE*

***Abstract*—In this paper, a novel preamble structure, including a synchronization field (S-field) and a cell-search field (C-field), is proposed for orthogonal-frequency-division-multiplexing-based cellular systems. An efficient algorithm for downlink synchronization and cell search using the preamble is also proposed. The synchronization and cell-search process includes the initial symbol-timing estimation using continuously or, at least, periodically transmitted downlink signal, the frame detection, the fine symbol-timing estimation, the frequency-offset estimation using the preamble S-field, and the cell identification using the preamble C-field. Performance of each synchronization and cell-search step is analyzed and verified by computer simulation. The overall performance of the synchronization and cell search is then analyzed in terms of the mean acquisition time. It is shown that the proposed preamble with the corresponding synchronization and cell-search algorithm can provide a very robust synchronization and cell-search capability, even in bad cellular environments.**

***Index Terms*—Cell search, cellular, orthogonal-frequency-division multiplexing (OFDM), preamble, synchronization.**

I. Introduction

RECENTLY, orthogonal-frequency-division multiplexing (OFDM) has been widely accepted as the most promising radio transmission technology for the next-generation wireless systems due to its advantages such as robustness to multipath fading, granular resource allocation capability, and no intracell interference. Among the conventional OFDM-based wireless systems, digital audio broadcasting, IEEE 802.11a, and Hiperlan/2 are well known [1]–[5]. For cellular systems, it is one of the most important requirements to provide robust synchronization and cell-search capability. For example, the wideband code-division multiple-access (WCDMA) system provides a hierarchical three-step cell search using the primary synchronization code and the secondary synchronization code in the synchronization channel (SCH) and the common pilot channel (CPICH) [6]. However, the synchronization schemes used in such conventional OFDM schemes are not appropriate for a cellular system since they cannot discriminate signals from different cells unless their carrier frequencies are different. Thus, devising a new synchronization and cell-search technique for OFDM-based cellular systems is required.

Recently, synchronization and cell-search techniques have been proposed for asynchronous OFDM–code-division-multiplexing cellular systems having a channel structure similar to the WCDMA [7], [8]. The differentially encoded SCH uses equally spaced subcarriers in every OFDM symbol and is common for every cell, while CPICH is spread by a cell-specific code in both the time and the frequency domains. However, asynchronous cellular systems generally suffer from longer cell-search time, particularly for a neighbor-cell search. Thus, synchronous cellular systems using the global positioning system (GPS) are considered to be more attractive for the next-generation cellular systems. In this paper, a novel preamble-based synchronization and cell-search technique for synchronous OFDM-based cellular systems using a novel preamble structure, which is comprised of a synchronization field (S-field) and a cell-search field (C-field), is proposed. The initial result of this work has been presented in [9]. The proposed preamble-based synchronization and cell search is fully analyzed, and the performance of the proposed algorithm is then verified by computer simulations in this paper. In addition, the overall performance of the proposed cell search is analyzed in terms of the mean acquisition time (MAT).

II. Proposed Preamble Structure

A. Design Motivation

In conventional OFDM-based wireless systems, such as IEEE 802.11a or Hiperlan/2, the functionality required for an initial synchronization includes signal detection, frame-timing estimation, and frequency-offset estimation. In order to achieve the above functionality, the most commonly used preamble structure in conventional OFDM-based wireless systems is to repeat a pattern, which is a sequence with a good autocorrelation property (autocorrelation function is close to the Kronecker delta function), a few times in a preamble symbol. Such a structure can provide a good time and frequency synchronization capability and has been successfully used in many commercial systems (see [5] and [11] for more detailed discussion).

Manuscript received April 19, 2005; revised April 5, 2006, November 30, 2006, and January 17, 2007. This work was supported in part by the MIC, Korea, under the ITRC support program supervised by the IITA under Grant IITA-2006-(C1090-0602-0011) and in part by the Ubiquitous Computing and Network (UCN) Project, MIC 21st Century Frontier R&D Program in Korea. The review of this paper was coordinated by Dr. E. Larsson.

K. S. Kim is with the Department of Electrical and Electronic Engineering, Yonsei University, Seoul 120-749, Korea (e-mail: ks.kim@yonsei.ac.kr).

S. W. Kim is with the Samsung Electronics Company, Ltd., Suwon 442-742, Korea.

Y. S. Cho is with the School of Electrical and Electronic Engineering, Chung-Ang University, Seoul 156-756, Korea.

J. Y. Ahn is with the Electronics and Telecommunications Research Institute, Daejeon 305-350, Korea.

Digital Object Identifier 10.1109/TVT.2007.901053

However, for a cellular system (in a single-frequency network as in commercial cellular systems), neighboring cells should use different preambles so that a mobile station can discriminate signals from different cells. Thus, the functionality required for the synchronization and cell search includes frame-timing estimation, frequency-offset estimation, and cell identification. Note that the signal detection is not required since a cellular system is not a burst transmission system. Once the cell number is obtained, a receiver can receive the broadcasting channel of the cell, and the whole cell information can be retrieved. A straightforward way to obtain the above functionality in an OFDM-based cellular system is to use different sequences, as many as the number of different cells, as the repetitive patterns of the preambles. Unfortunately, such a preamble design results in a formidable complexity of the synchronization and cell search (the number of candidates is the number of samples in a frame times the number of different cells). Thus, a preamble structure for a cellular system should not only provide robust capability of synchronization and cell search but also enable us to use a low-complexity hierarchical synchronization and cell-search algorithm. Thus, the motivation of the proposed preamble design is as follows.

1) It should provide an acceptable acquisition time even in a very bad cellular environment where the mobile speed is quite fast and the average signal-to-noise ratio (SNR) is very low.
2) It should allow a low-complexity hierarchical algorithm.

B. Preamble Design

The rough structure of the proposed preamble to obtain the functionality and to meet the design motivation described in Section II-A can be determined from the following observations.

1) In a synchronous system, base stations can transmit a common preamble for the timing-estimation stage, and the received signal is equivalent to the signal from a single transmitter through a multipath channel.
2) We can ignore the relative frequency offset between different base stations in a GPS-aided synchronous system.
3) In order to identify the cell number, the signals from different base stations should be as different as possible.

Based on the above observations, we determine to use two different components, which are denoted as the preamble S-field and the preamble C-field, for the proposed preamble structure. The preamble S-field is common for all base stations and is used for the frame-timing estimation and the frequency-offset estimation. The detailed requirements and the design approach of the preamble S-field are as follows.

1) To reduce the complexity of the cell identification, the integral part of the frequency offset should be estimated. This requirement can be fulfilled by using a repetitive pattern in the preamble S-field.
2) A reliable frame-timing estimation can be fulfilled by designing the above repetitive pattern in the preamble S-field to have a good autocorrelation property.
3) A natural way to perform a low-complexity hierarchical estimation is as follows:
   a) estimating a rough symbol timing;
   b) determining the location of the S-field symbol;
   c) estimating the exact frame timing.
4) Step a) above can easily be done using the cyclic prefix (CP). In addition, Step c) can be done using the autocorrelation property of the S-field. Thus, the remaining task is to give the S-field a unique structure that differentiates the S-field from other ordinary OFDM symbols. This can be fulfilled by using the inverted postfix structure of the S-field.

The preamble C-field is used for the cell-number identification, and each cell with a different cell number uses a different preamble C-field. Then, the detailed requirements and the design approach of the preamble C-field are as follows.

1) The best way to make OFDM signals is to use different subcarriers. Thus, the C-fields of adjacent cells should use different sets of subcarriers.
2) To increase the number of different cells, the different cells (not adjacent) may use the same set of subcarriers with different sequences (with a good cross-correlation property) on these subcarriers.
3) Even to accommodate a higher number of different cells, the C-field can be comprised of more than one OFDM symbol.

The detailed preamble design from the above design strategy is as follows. The downlink frame structure considered in this paper and the proposed preamble structure (both in the time and the frequency domains) are shown in Fig. 1. A preamble, with length T_p, is located at the beginning of the frame and is followed by a number of data slots, where pilot symbols are well spread both in the time and the frequency domains. The length of the S-field is T_{ps}, which is equal to the OFDM symbol duration T_s. The S-field signal is composed of one S symbol and one IS' symbol. The IS' symbol is the first T_{CP}-length part of the π-phase-rotated version of the S symbol, and the S symbol is comprised of $N_{S\mathrm{sym}}$ repetitive S_a symbols. Here, T_{CP} is the length of the CP. As shown in Fig. 1, one good example of the preamble S-field signal $P_S(t)$ is

$$P_S(t) = \begin{cases} \sum_{k=0}^{N_F-1} g(k)\varphi_k(t), & 0 \le t < T_d \\ -\sum_{k=0}^{N_F-1} g(k)\varphi_k(t-T_d), & T_d \le t < T_{ps} \\ 0, & \text{otherwise} \end{cases} \quad (1)$$

where N_F is the size of the fast Fourier transform (FFT), $\varphi_k(t) = \exp(-j2\pi(k-N_F/2)t/T_d))$, $T_d = T_s - T_{\mathrm{CP}}$, $g(k) = \mu(i)\delta_{\mathrm{K}}(k - iN_{S\mathrm{sym}})$, $\mu(i)$ is a pseudorandom sequence such as the m-sequence, and $\delta_{\mathrm{K}}(\cdot)$ is the Kronecker delta function. Since nonzero symbol values are assigned at every $N_{S\mathrm{sym}}$ subcarrier in (1), the S symbol has $N_{S\mathrm{sym}}$ repetitive patterns (each is denoted as the S_a symbol). Among the many possible S-field signals given by (1), the signal with a low peak-to-average power ratio and a good correlation property can be selected as the preamble S-field.

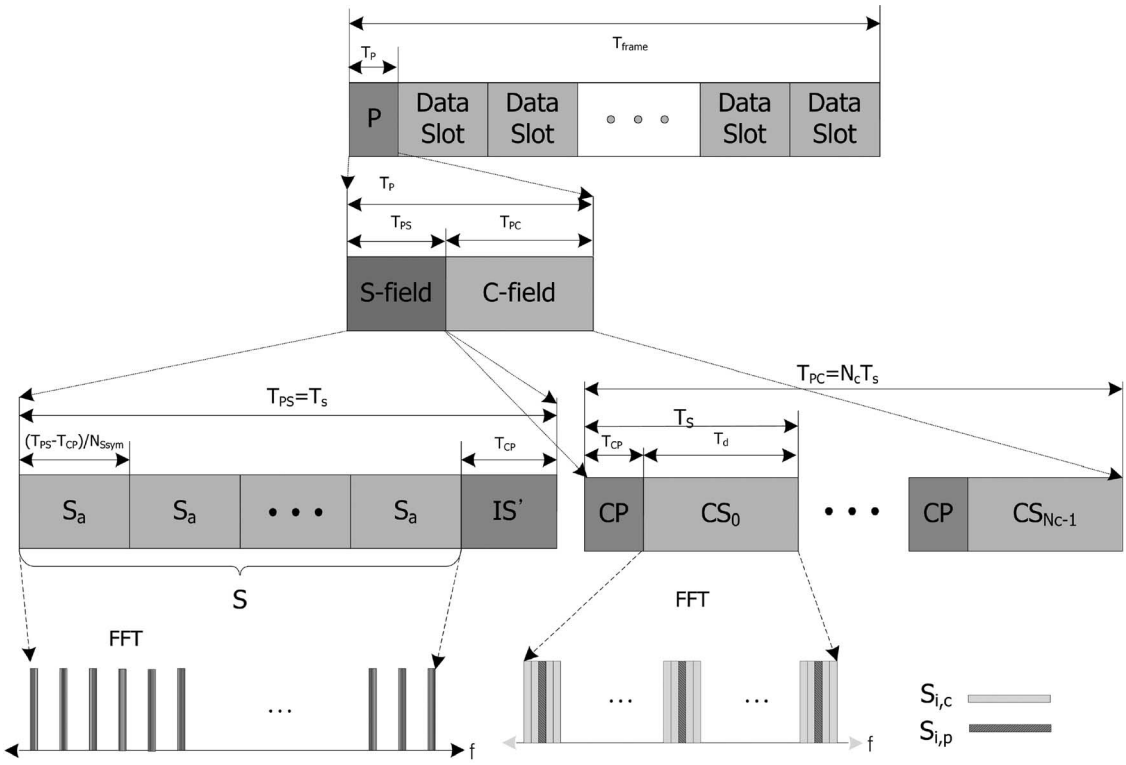

Fig. 1. Abstract downlink frame structure and the proposed preamble structure.

The length of the C-field is equal to N_cT_s. The C-field signal of the mth cell $P_C^m(t)$ is defined as

$$P_C^m(t) = \begin{cases} \sum_{k=0}^{N_F-1} c_n^m(k)\varphi_k(t+T_d-T_{\mathrm{CP}}), & 0 \le t-nT_s < T_{\mathrm{CP}} \\ \sum_{k=0}^{N_F-1} c_n^m(k)\varphi_k(t-T_{\mathrm{CP}}), & T_{\mathrm{CP}} \le t-nT_s < T_s \\ 0, & \text{otherwise} \end{cases} \tag{2}$$

where $c_n^m(k)$, $0 \le n \le N_c-1$, is the frequency-domain signal at the kth subcarrier of the nth symbol of the C-field of the mth cell. The construction of $c_n^m(k)$ is as follows.

1) Let $S = \{s_0, s_1, \ldots, s_{P-1}\}$ be a set of partitions of all used subcarriers. Furthermore, the ith partition s_i is divided into $s_{i,p}$ and $s_{i,c}$.
2) Let $\psi_{i,j}$, $i = 0, \ldots, P-1$, $j = 0, \ldots, G-1$, be the sequences with good correlation properties and $\bar{\psi}$ be a sequence used for known pilot-symbol pattern.
3) For each symbol of the C-field, there are P different partitions and G different sequences. Thus, $M = PG$ different symbols are prepared.
4) Let p_n and q_n be the partition number and the sequence number for the nth symbol of the C-field, respectively. Then, the cell number m is determined by the combination of the N_c partition numbers $(p_0, \ldots, p_{N_c-1})$ and the N_c sequence numbers $(q_0, \ldots, q_{N_c-1})$ as

$$m = \sum_{n=0}^{N_c-1} (p_nG + q_n)M^n. \tag{3}$$

5) Finally, $c_n^m(k)$ is defined as

$$c_n^m(k) = \begin{cases} \psi_{p_n,q_n}(j), & k = s_{p_n,c}(j) \\ \bar{\psi}(j), & k = s_{p_n,p}(j) \\ 0, & \text{otherwise} \end{cases} \tag{4}$$

where $\psi_{p_n,q_n}(j)$, $\bar{\psi}(j)$, $s_{p_n,p}(j)$, and $s_{p_n,c}(j)$ denote the jth elements of ψ_{p_n,q_n}, $\bar{\psi}$, $s_{p_n,p}$, and $s_{p_n,c}$, respectively.

Here, we can see that, with the proposed C-field, M^{N_c} different cells can be discriminated. As an example, let $N_c = 2$, $P = 8$, and $G = 8$. Then, the number of cells that can be discriminated is $M^{N_c} = 64^2 = 4096$, which is large enough for a cellular system.

C. Comparison With the IEEE802.16e Preamble Structure

Among the recently developed OFDM-based wireless systems, IEEE802.16e [10] OFDMA physical layer adopted 114 different preamble patterns by using cell-specific sequences transmitted over one of the three frequency partitions called segments. In addition, an optional common synchronization preamble can be used at the end of the downlink frame structure for simpler timing estimation in which a pseudorandom code is transmitted on even-numbered subcarriers (two repetitive patterns in the time domain) with an ordinary CP. The advantage of the proposed preamble structure can be summarized as follows.

1) The inverted postfix structure of the proposed preamble (IS' symbols) is a very unique structure that enables us to find the beginning point of a frame without a fine timing estimation. With the proposed preamble structure,

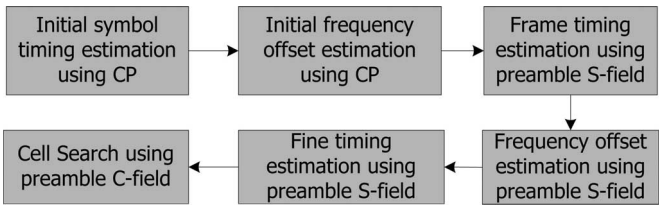

Fig. 2. Proposed synchronization process.

a low-complexity hierarchical synchronization algorithm similar to that in WCDMA [6] can be applied.

2) The main preamble structure of IEEE802.16e can be considered as a special case of the proposed C-field.
3) Additional advantages of the proposed C-field are as follows.
   a) Many more different cells can be implemented by allowing more than one OFDM symbol for the preamble C-field if necessary.
   b) The proposed C-field allows a flexible form of partitions.
   c) Performance can be improved by coherently combining whole symbols with the aid of the known pilot sequence in the proposed C-field, provided that channel estimation is reliable. In addition, when the proposed C-field uses a partition comprised of distributed clusters (adjacent subcarriers in a cluster), as shown in Fig. 1, the symbols within a cluster can be coherently combined without channel estimation.

Thus, it is apparent that we can easily reduce the complexity of the synchronization and cell search, which is critical for a mobile station. In addition, we can expect that the cell-identification performance of the proposed preamble is better when both preambles use the same number of subcarriers since the proposed preamble allows coherent combining.

III. Synchronization

In Fig. 2, the synchronization process proposed in this paper is shown. In the conventional OFDM-based systems such as wireless LAN, all of the initial synchronization processes, including signal detection, are performed using the preamble [11]. However, in an OFDM-based cellular system employing frequency-division multiplexing (FDD), signals are transmitted continuously or, at least, periodically due to the common pilot symbols and common channels used for broadcasting. By taking these into account, we can devise a more efficient hierarchical synchronization and cell-search algorithm. First, the signal-detection step is not required in the synchronization of OFDM-based cellular systems using FDD. In addition, a symbol-timing acquisition within a certain range (roughly speaking, 10%–20% of the length of the CP, which corresponds to 1 dB–2 dB SNR loss) is enough for the cell search. Thus, as the first step of the synchronization and cell search, an initial symbol timing and an initial frequency offset are obtained using a simple CP-based methods such as in [12] and [13]. Note that the required length of the searching window in the initial symbol-timing estimation is at most over an OFDM-symbol period. After achieving the initial synchronization, we can estimate the frame timing using the novel structure of the preamble S-field. As will be seen later, we evaluate a metric for the frame-timing estimation at the sample point obtained from the initial symbol-timing estimation for each OFDM symbol. Thus, the number of candidates in the frame-timing estimation is at most the number of OFDM symbols in a frame. Thus, the proposed hierarchical synchronization scheme has much lower complexity than the conventional synchronization schemes [11], [14]–[16]. Although the fine timing estimation is not an essential task required for a cell search, it is eventually required for successful data reception. Thus, a fine timing estimation is performed using the preamble S-field after the frame timing is obtained. In this paper, a cross-correlation-based method [11], [17] is adopted with a timing back-off for better performance [18]. Finally, frequency-offset estimation is performed by applying an autocorrelation-based method, such as in [11] and [19], to the repetitive structure of the preamble S-field.

A. Initial Symbol Timing and Frequency-Offset Estimation

Let the sampled received signal be $y(n)$ and $z(k)$ be

$$z(k) = \frac{1}{N_{\mathrm{CP}}} \sum_{r=0}^{N_{\mathrm{CP}}-1} y^*(k+r)y(k+r+N_F) \tag{5}$$

where N_{CP} is the number of samples in the CP. Then, the initial symbol timing τ_{init} is obtained using the CP correlation as [12]

$$\tau_{\mathrm{init}} = \arg\max_n \left| \sum_{j=0}^{N_{\mathrm{init}}-1} z(n+jN_s) \right| \tag{6}$$

where N_s and N_{init} are the number of samples in an OFDM symbol and the number of OFDM symbols used in the initial symbol-timing estimation, respectively. In addition, we can estimate the initial frequency offset ϵ_{init} as [12]

$$\epsilon_{\mathrm{init}} = \frac{1}{2\pi} \arg\left\{ \sum_{j=0}^{N_{\mathrm{init}}-1} z(\tau_{\mathrm{init}}+jN_s) \right\}. \tag{7}$$

Note that (7) can estimate only the fractional part of the frequency offset (normalized by the subcarrier spacing). The estimation of the integral part of the frequency offset will be taken care of using the preamble S-field.

B. Frame-Timing Estimation

After obtaining the initial synchronization, we have $N_f (= T_{\mathrm{frame}}/T_s)$ candidates for the frame timing. Here, we utilize the property of the preamble S-field where every OFDM symbol, except the preamble S-field, has a positive value of autocorrelation due to the CP, while the preamble S-field has a negative value of autocorrelation due to the inverted postfix structure. By exploiting the unique structure of the preamble S-field, the frame timing is estimated as

$$\begin{aligned} \tau_f(\iota) &= \iota N_s + \tau_{\mathrm{init}}, && 0 \le \iota < N_f \\ \tau_{\mathrm{frame}} &= \tau_f(\iota), && \text{if } \Re\{z_c(\tau_f(\iota))\} < 0 \end{aligned} \tag{8}$$

where $\Re\{x\}$ is the real part of x, and $z_c(\cdot)$ in (8) is the same as (5), except that the received samples after frequency-offset compensation with the initial frequency-offset estimate obtained in (7) $y_c(\cdot)$ is used instead of $y(\cdot)$. For better frame-timing estimation performance, one may use $\tau_{\text{frame}} = \min_\iota \Re\{z_c(\tau_f(\iota))\}$ instead of using (8), particularly when SNR is low. However, this will cause additional delay since the observation window should be at least one frame, which may degrade the performance of the whole cell-search process in terms of the MAT.

C. Fine Symbol-Timing Estimation

In the case where the frequency offset have both the integral and the fractional parts, the frequency offset ϵ_f can be estimated using the repetitive property of the preamble S-field as [11], [19]

$$\epsilon_f = \frac{N_{S\text{sym}}}{2\pi} \arg\left\{ \sum_{r=0}^{N_{\text{CP}}-1} y^*(\tau_s+r) y(\tau_s+r+N_F/N_{S\text{sym}}) \right\}. \tag{9}$$

Note that (9) can estimate the normalized frequency offset in the range of $[-N_{S\text{sym}}/2, N_{S\text{sym}}/2]$.

After obtaining the frame timing, we can assume that the starting point of the preamble S-field is around the estimated frame timing τ_{frame}. Then, we can estimate the fine symbol timing τ_s with the timing backoff by taking the cross correlation between the frequency-offset compensated signal $y_c(\cdot)$ with the result obtained in (9) and the preamble S-field signal as [11], [17]

$$\tau_s = \arg\max_n \left| \sum_{r=0}^{R-1} P_S^*(r+R_s) y_c(n+r+R_s) \right| - N_B \tag{10}$$

where $P_S(r)$ is the sampled signal of the preamble S-field, R is the number of samples used for the fine symbol-timing estimation, R_s is the starting point for accumulation, and N_B is the number of samples for the timing back-off. In OFDM systems, a negative timing error (estimated timing is greater than true timing) causes intersymbol-interference (ISI) and interchannel-interference (ICI) effects, while a small positive timing error (less than the CP length minus the channel delay) does not. Thus, we can reduce the ISI and the ICI effects by introducing an appropriate timing backoff.

D. Performance Analysis

Let $h(t) = \sum_{l=0}^{L-1} h_l \delta(t - \tau_l^c)$ be the channel impulse response and $x(k)$ be the sampled transmitted signal with average power P_x/N_F. Assuming that the frequency-offset estimation is perfect, the received signal after sampling with sampling period T and frequency-offset compensation is given by

$$y(k) = \sum_{l=0}^{L-1} h_l x(k-\tau_l) + n(k) \tag{11}$$

where τ_l, which is defined by τ_l^c/T, is assumed to be an integer. For notational simplicity, we use y instead of y_c. In addition, $\tau_0 = 0$ and $k = 0$ represent the frame boundary without loss of generality. The complex channel gain of the lth path h_l is assumed to be a complex Gaussian process with mean zero and variance β_l (i.e., Rayleigh fading channel). Moreover, $n(k)$ is assumed to be a complex Gaussian process with mean zero and variance $2\sigma_n^2$. Define

$$\zeta(k) = \frac{1}{R} \sum_{r=0}^{R-1} x^*(r) y(k+r). \tag{12}$$

In the case where N_{CP} is sufficiently large, which is true for most OFDM cellular systems due to the large delay spread of outdoor environments, we can assume that $z(k)$ and $\zeta(k)$ are Gaussian random processes with means $m_z(k)$ and $m_\zeta(k)$ and variances $2\sigma_z^2(k)$ and $2\sigma_\zeta^2(k)$, respectively, using the central limit theorem (CLT). The statistics can be summarized as

$$\begin{aligned} m_z(k) &\cong (-1)^{\delta_{\text{K}}(\lfloor k/N_s \rfloor)} \frac{P_x q(k) \kappa}{N_F} \\ \sigma_z^2(k) &\cong \frac{2\sigma_n^2 P_x \kappa}{N_{\text{CP}} N_F} + \frac{2\sigma_n^4}{N_{\text{CP}}} \\ m_\zeta(k) &= \frac{P_x}{N_F} \sum_{l=0}^{L-1} h_l \delta_{\text{K}}(k-\tau_l) \\ \sigma_\zeta^2(k) &\cong \frac{P_x^2 \kappa}{2RN_F^2} + \frac{\sigma_n^2 P_x}{RN_F} \end{aligned} \tag{13}$$

where $\kappa = \sum_{l=0}^{L-1} |h_l|^2$, and $\lfloor x \rfloor$ is the greatest integer not exceeding x. Here, $q(k) = \max(0, 1 - (u(k)/N_{\text{CP}}))$ denotes the loss due to the initial timing-estimation error, where $u(k) = |k - N_s \cdot \lfloor k/N_s + 1/2 \rfloor|$ represents the distance to the nearest OFDM-symbol starting point from k. Derivations are given in Appendix A.

1) Initial Synchronization: The outage probability of the initial symbol timing $\Pr\{|\tau_{\text{init}}| > \tau_{\text{th}}\}$ can be calculated from the statistic of $z(k)$ by using a numerical method for a given threshold τ_{th}. In addition, the outage probability of the initial symbol-timing estimation can be reduced by increasing N_{init}. In the sequel, we assume that the initial timing estimation is successful with the initial timing error equals to τ_{init}. Furthermore, we assume that the frequency offset is well estimated so that the effect of the remaining frequency offset in the following synchronization and cell-search procedure can be ignored.

2) Frame-Timing Estimation: If the transmitted symbol is not the preamble S-field, i.e., $\iota \neq 0$, it can be easily seen from (8) and the statistic of $z(k)$ that the false-alarm probability of frame detection conditioned on the combined fading channel gain (κ) $P_{\text{fa,frame}}(\kappa)$ is given by

$$\begin{aligned} P_{\text{fa,frame}}(\kappa) &= \Pr\{\Re\{z(\iota N_s + \tau_{\text{init}}) < 0\} \\ &\cong Q\left(\sqrt{\frac{2g\gamma^2\kappa^2}{2\gamma\kappa+1}} \right) \end{aligned} \tag{14}$$

where $\gamma = P_x/(2\sigma_n^2 N_F)$, $g = q^2(\tau_{\text{init}}) N_{\text{CP}}$, and $Q(x) = (1/\sqrt{2\pi}) \int_x^\infty \exp(-t^2/2) dt$. On the other hand, if the transmitted symbol is the preamble S-field, i.e., $\iota = 0$, the

detection-failure probability conditioned on the combined fading channel gain (κ) $P_{\mathrm{df,frame}}(\kappa)$ is given by

$$P_{\mathrm{df,frame}}(\kappa) = \Pr\{\Re\{z(\tau_{\mathrm{init}}) > 0\} \cong Q\left(\sqrt{\frac{2g\gamma^2\kappa^2}{2\gamma\kappa+1}}\right). \quad (15)$$

Note that (15) is identical to (14) because $m_z(\tau_{\mathrm{init}}) = -m_z(\iota N_s + \tau_{\mathrm{init}})$, and $\sigma_z^2(\tau_{\mathrm{init}}) = \sigma_z^2(\iota N_s + \tau_{\mathrm{init}})$ for $\iota \neq 0$.

3) Fine Symbol-Timing Estimation: Although the fine symbol-timing estimation is not an essential part for the cell search, it is required for the good quality of data reception. In addition, it is not only required for the initial cell search but also required for the time tracking in an OFDM cellular system. Thus, it is required to analyze the performance of the fine symbol-timing estimation separately from the cell search in fading channels. In previous literature such as [15] and [18], the mean-square error has been used for a performance measure. In this paper, however, the probability that the ISI and the ICI occur due to the falsely estimated symbol timing is used as a performance measure for the fine symbol-timing estimation. Since the ISI and the ICI occur when a nonnegligible path exists before the start point of the FFT window at the receiver, we can define the timing-error probability $P_{e,\mathrm{timing}}$ as

$$P_{e,\mathrm{timing}} = \Pr\left\{\max_{k\in K_s}|\zeta(k)|^2 < \max_{k\in K_f}|\zeta(k)|^2\right\} \quad (16)$$

where $K_s = \{k|0 \le k < N_B\}$, $K_f = \{k|-N_w/2 \le k < N_w/2, k \notin K_s\}$, and N_w is the search window size of the fine symbol-timing estimation. Here, we assume that $-(N_w/2) \le \tau_{\mathrm{init}} < (N_w/2)$ and that the frame-timing estimation is successful. Let U_s be the set given by $\{\tau_0, \ldots, \tau_{L(N_B)-1}\}$. Here, $L(N_B)$ denotes the largest integer such that $\tau_{L(N_B)-1} < N_B$. If we set N_B to be sufficiently large so that $\beta_l \ll \beta_0$ for $l \ge L(N_B)$, we can further approximate $|\zeta(k)|^2$, $k \in K_f$ as an independent and identical central chi-square random process and $\max_{k\in U_s}|\zeta(k)|^2 \cong \max_{k\in K_s}|\zeta(k)|^2$. Then, as derived in Appendix B, the timing-error probability is given by

$$\begin{aligned} P_{e,\mathrm{timing}} &\cong \Pr\left\{\max_{k\in U_s}|\zeta(k)|^2 < \max_{k\in K_f}|\zeta(k)|^2\right\} \\ &\cong E\left\{\Pr\left\{|\zeta(\tau_l)|^2 < \max_{k\in K_f}|\zeta(k)|^2 \,|l = \arg\max_{0\le l<L(N_B)}|h_l|\right\}\right\} \\ &= 1 - \sum_{n=1}^{L(N_B)}\sum_{v\in V_n}(-1)^{n+1}\frac{v^T w}{R\gamma + v^T w} \\ &\quad \times B\left(N_w - N_B + 1, \frac{v^T w}{R\gamma + v^T w}\right) \end{aligned} \quad (17)$$

where v is the $L(N_B)\times 1$ column vector whose elements are either zero or one. In addition, w is defined by $[\beta_0^{-1}\beta_1^{-1}\cdots\beta_{L(N_B)-1}^{-1}]^{\mathrm{T}}$, V_n is the collection of all v's consisting of n elements of "one," and $B(x,y)$ is the beta function [20].

IV. Cell Identification

For the cell identification, we need to estimate the partition numbers p_n, $n = 1, \ldots, N_c$ and the sequence numbers q_n, $n = 1, \ldots, N_c$, which are used to generate the preamble C-field. In this paper, we consider a hierarchical cell-identification algorithm for low computational complexity. For each OFDM symbol in the preamble C-field, the partition number is estimated by calculating the received signal power contained in each partition and choosing the partition with the largest power. Then, the sequence number is estimated by comparing cross-correlation values between candidate sequences and the received frequency symbols on the selected partition. Finally, we obtain the cell number from the estimated partition numbers and the estimated sequence numbers of the N_c OFDM symbols in the preamble C-field.

A. Cell-Identification Algorithm

Let $Y_n(k)$ be the received frequency-domain symbol at the kth subcarrier in the nth OFDM symbol. Then, for the nth symbol of the preamble C-field, the subcarrier partition number p_n can be estimated as

$$\hat{p}_n = \arg\max_p \sum_{k\in s_p}|Y_n(k)|^2. \quad (18)$$

Let $H(k) = \sum_{l=0}^{L-1} h_l \exp(-j2\pi\tau_l k/N_F)$ be the complex channel at the kth subcarrier. Then, from the received frequency-domain symbols $Y_n(k)$, $k \in s_{\hat{p}_n,p}$, and the known pilot sequence $\bar{\Psi}$, the estimated channel gain $\hat{H}(k)$ can be obtained by applying an appropriate channel-estimation scheme such as the modified least-squares estimator [21]. Let $\chi_{p,q}$ be the cross correlation between the channel-compensated symbols in the subcarrier set s_p and the sequence $\psi_{p,q}$, which is defined by

$$\chi_{p,q} = \sum_{j=0}^{|s_{p,c}|-1} Y_n(s_{p,c}(j))\,\hat{H}^*(s_{p,c}(j))\,\psi_{p,q}^*(j) \quad (19)$$

where $|A|$ denotes the cardinality of a set A. Then, the sequence number of the nth symbol of the preamble C-field q_n can be estimated as

$$\hat{q}_n = \begin{cases} \arg\max_q \Re\{\chi_{\hat{p}_n,q}\}, & \chi_{\hat{p}_n,\hat{q}_n} > \chi_{\mathrm{th}} \\ \text{Detection fails}, & \text{otherwise} \end{cases} \quad (20)$$

where χ_{th} is the threshold for the cell identification. Finally, the cell number is estimated as

$$\hat{m} = \sum_{n=0}^{N_c-1}(\hat{p}_n G + \hat{q}_n)M^n. \quad (21)$$

B. Performance Analysis of the Partition Estimation

Although the proposed algorithm can be applied for any value of N_c, any partition set S, and any sequence sets $\psi_{i,j}$, $i = 0, \ldots, P-1$, $j = 0, \ldots, G-1$, we consider a simple but

useful example for the performance analysis of the partition estimation and the sequence estimation shown in this and the next sections as follows.

1) Assume that we use all of the subcarriers for simplicity.
2) Let $\lambda(N_{fs}, d)$, $0 \le d < N_{fs}$ be the dth comb set of subcarriers with spacing N_{fs} (the set of equally spaced subcarriers starting from the dth subcarrier with spacing N_{fs}) defined as
$$\lambda(N_{fs}, d) = \{k | k \bmod N_{fs} = d, 0 \le k < N_F - 1\}.$$
3) Here, we choose N_{fs} so that $D = N_{fs}/P$ and $N_{fn} = N_F/N_{fs}$ are integers.
4) The ith partition s_i is composed of D consecutive comb sets, i.e., $s_i = \cup_{d=0}^{D-1} \lambda(N_{fs}, iD + d)$.
5) In every partition, one comb set located at the center is used for transmitting pilot sequence, i.e., $s_{i,p} = \lambda(N_{fs}, iD + \lfloor D/2 \rfloor)$.
6) The magnitude of each element in any sequence is one, i.e., $|\psi_{p,q}(j)| = 1, \forall j$.

Then, for the nth OFDM symbol of the preamble C-field, the partition number is estimated as

$$\begin{aligned}\hat{p}_n &= \arg\max_p \sum_{k \in s_p} |Y_n(k)|^2 \\ &= \arg\max_p Z(p) \end{aligned} \tag{22}$$

where

$$Z(p) = \sum_{r=0}^{N_{fn}-1} \sum_{d=0}^{D-1} |Y_n(rN_{fs} + pD + d)|^2 . \tag{23}$$

Let the cell number and the corresponding partition number in the nth preamble C-field symbol be m and p_n, respectively. Then, the received symbol in the frequency domain $Y_n(k)$ is given by

$$Y_n(k) = \sqrt{\frac{P_x P}{N_F}} H(k) c_n^m(k) + N(k) \tag{24}$$

where $N(k)$ is a complex Gaussian noise with mean zero and variance $2\sigma_n^2$. Note that each frequency-domain symbol of the preamble C-field is boosted by the factor of P. Since $c_n^m(k) \neq 0$ only for $k \in s_{p_n}$ in (24), it is easily seen that $Z(p), p \neq p_n$, is a central chi-square random variable with the degree of $2DN_{fn}$, and $Z(p_n)$ is a noncentral chi-square random variable with the degree of $2DN_{fn}$ and the noncentrality parameter of $\sum_{d=0}^{D-1} \xi_d$, where

$$\begin{aligned}\xi_d &= \frac{P_x P}{N_F} \sum_{r=0}^{N_{fn}-1} |H(rN_{fs} + pD + d)|^2 \\ &= \frac{P_x P}{N_F} \sum_{r=0}^{N_{fn}-1} \sum_{l_1=0}^{L-1} \sum_{l_2=0}^{L-1} h_{l_1} h_{l_2}^* \\ &\quad \times \exp\left(-\frac{j2\pi(\tau_{l_1} - \tau_{l_2})(rN_{fs} + pD + d)}{N_F} \right) \\ &= \frac{P_x P}{N_F} \sum_{l_1=0}^{L-1} \sum_{l_2=0}^{L-1} h_{l_1} h_{l_2}^* \exp\left(-\frac{j2\pi(pD + d)(\tau_{l_1} - \tau_{l_2})}{N_F} \right) \\ &\quad \times \sum_{r=0}^{N_{fn}-1} \exp\left(-\frac{j2\pi(\tau_{l_1} - \tau_{l_2})r}{N_{fn}} \right) \\ &= \frac{P_x P}{N_F} N_{fn} \kappa \end{aligned} \tag{25}$$

is the signal power contained in the dth comb set. Here, the last equality in (25) comes from the assumption for simplicity that $\tau_i - \tau_j$ is not an integer multiple of N_{fn} for $0 \le i \neq j < L$. Then, using the results in [22], we obtain an upper bound on the partition estimation error $P_{e,\mathrm{part}}(\kappa)$ as

$$\begin{aligned} P_{e,\mathrm{part}}(\kappa) &= \Pr\{\hat{p}_n \neq p_n | \kappa\} \\ &\le \frac{P-1}{2^{2N_F/P-1}} \exp\left(-\frac{N_F \gamma \kappa}{2} \right) \\ &\quad \times \sum_{r=0}^{N_F/P-1} C(N_F/P, r) \left(\frac{N_F \gamma \kappa}{2} \right)^r \end{aligned} \tag{26}$$

where $C(w, r) = (1/r!) \sum_{k=0}^{w-r-1} \binom{2w-1}{k}$.

C. Performance Analysis of the Sequence Estimation

Let us assume that the channel estimation is perfect so that $\hat{H}(k) = \sqrt{(P_x P/N_F)} H(k)$ and the sequences are independent binary random codes. Then, from Appendix C, we can assume that $\Re\{\chi_{p,q}\}$ is a Gaussian random variable whose mean and variance are

$$\begin{aligned} m_{\chi_{p,q}} &= E\{\Re\{\chi_{p,q}\}\} \\ &= \begin{cases} \frac{P_x P}{N_F}(D-1)N_{fn}\kappa, & p = p_n, q = q_n \\ 0, & \text{otherwise} \end{cases} \end{aligned} \tag{27}$$

and

$$\begin{aligned} \sigma^2_{\chi_{p,q}} &= \mathrm{Var}\{\Re\{\chi_{p,q}\}\} \\ &= \begin{cases} \frac{2P_x^2 P^2 (D-1) N_{fn} \kappa^2}{N_F^2} + \frac{P_x P \sigma_n^2 (D-1) N_{fn} \kappa}{N_F}, & p = p_n, q \neq q_n \\ \frac{P_x P \sigma_n^2 (D-1) N_{fn} \kappa}{N_F}, & \text{otherwise} \end{cases} \end{aligned} \tag{28}$$

respectively. Here, we set χ_{th} as $\sqrt{\varepsilon} m_{\chi_{p_n,q_n}}$, where ε is a predetermined constant between zero and one. In practice, the threshold could be estimated during the partition estimation process. For example, χ_{th} may be chosen as

$$\chi_{\mathrm{th}} = \frac{\sqrt{\varepsilon}(D-1)}{D} \times \left[\sum_{k \in s_{\hat{p}_n}} |Y_n(k)|^2 - \frac{1}{P-1} \sum_{k \notin s_{\hat{p}_n}} |Y_n(k)|^2 \right]. \tag{29}$$

When the frame detection is erroneous, the sequence estimation is done with an OFDM symbol that is not a preamble C-field. If we assume that the OFDM symbol is sent with power P_x and that the frequency symbols are independent and identically distributed (i.i.d.) complex random variables with

zero mean, the statistic of $\chi_{p,q}$ is the same as that of $\chi_{p_n,q}$, $q \neq q_n$ given in (C4), except that the $i_{\chi_{p_n,q}}$ term in (C4) is complex and P times smaller in power. Thus, we have $\mathrm{Var}\{\Re\{\chi_{p,q}\}\} = ((P_x^2 P(D-1)N_{fn}\kappa^2)/N_F^2) + ((P_x P\sigma_n^2(D-1)N_{fn}\kappa)/N_F)$. Then, the false-alarm probability and the detection-failure probability when the frame detection is erroneous, which are $P_{\mathrm{fa1}}(\kappa)$ and $P_{\mathrm{df1}}(\kappa)$, respectively, are given as

$$\begin{aligned} P_{\mathrm{fa1}}(\kappa) &= \Pr\left\{\max_q \Re\{\chi_{p_n,q}\} > \chi_{\mathrm{th}}\right\} \\ &= 1 - \left(\Pr\left\{\Re\{\chi_{p_n,q}\} < \chi_{\mathrm{th}}|\kappa\right\}\right)^G \\ &= 1 - \left(1 - Q\left(\sqrt{\frac{2\varepsilon\gamma P(D-1)N_{fn}\kappa}{2\gamma\kappa+1}}\right)\right)^G \\ P_{\mathrm{df1}}(\kappa) &= 1 - P_{\mathrm{fa1}}(\kappa). \end{aligned} \tag{30}$$

Strictly speaking, P_{df1} should not be called the detection-failure probability since the sequence estimation is not performed with the preamble in this case. However, we will denote it as the detection-failure probability in this paper for notational simplicity.

The false-alarm probability and the detection-failure probability when the frame detection is correct but the partition estimation is erroneous, $P_{\mathrm{fa2}}(\kappa)$ and $P_{\mathrm{df2}}(\kappa)$, respectively, are given as

$$\begin{aligned} P_{\mathrm{fa2}}(\kappa) &= \Pr\left\{\max_q \Re\{\chi_{p,q}\} > \chi_{\mathrm{th}}, p \neq p_n\right\} \\ &= 1 - \Pr\left\{\Re\{\chi_{p,q}\} < \chi_{\mathrm{th}}, p \neq p_n|\kappa\right\}^G \\ &= 1 - \left(1 - Q\left(\sqrt{2\varepsilon\gamma P(D-1)N_{fn}\kappa}\right)\right)^G \\ P_{\mathrm{df2}}(\kappa) &= 1 - P_{\mathrm{fa2}}(\kappa). \end{aligned} \tag{31}$$

Finally, the false-alarm probability when the frame detection and the partition estimation are correct $P_{\mathrm{fa3}}(\kappa)$ is given as

$$\begin{aligned} P_{\mathrm{fa3}}(\kappa) &= \Pr\left\{\max_{q,q\neq q_n} \Re\{\chi_{p_n,q}\} > \max(\chi_{p_n,q_n}, \chi_{\mathrm{th}})\right\} \\ &= \Pr\left\{\max_{q,q\neq q_n} \Re\{\chi_{p_n,q}\} > \chi_{\mathrm{th}}, \Re\{\chi_{p_n,q_n}\} < \chi_{\mathrm{th}}\right\} \\ &\quad + \Pr\left\{\max_{q,q\neq q_n} \Re\{\chi_{p_n,q}\} > \Re\{\chi_{p_n,q_n}\} > \chi_{\mathrm{th}}\right\} \\ &= \left(1 - \left(1 - Q\left(\sqrt{\frac{2\varepsilon\gamma P(D-1)N_{fn}\kappa}{4\gamma P\kappa+1}}\right)\right)^{G-1}\right) \\ &\quad \times Q\left(\sqrt{2\gamma P(D-1)N_{fn}(1-\sqrt{\varepsilon})^2\kappa}\right) \\ &\quad + \frac{1}{\sqrt{2\pi\sigma_{\chi_{p_n,q_n}}}} \int_{\chi_{\mathrm{th}}}^{\infty} \left(1 - \left(1 - Q\left(\frac{y}{\sigma_{\chi_{p_n,q}}}\right)\right)^{G-1}\right) \\ &\quad \times \exp\left(-\frac{(y - m_{\chi_{p_n,q_n}})^2}{2\sigma_{\chi_{p_n,q_n}}}\right) dy \end{aligned} \tag{32}$$

where the second term can be obtained from numerical integration. $P_{\mathrm{fa3}}(\kappa)$ in (32) can be further approximated as

$$\begin{aligned} P_{\mathrm{fa3}}(\kappa) &\cong (G-1)Q\left(\sqrt{\frac{2\varepsilon\gamma P(D-1)N_{fn}\kappa}{4\gamma P\kappa+1}}\right) \\ &\quad \times Q\left(\sqrt{2\gamma(D-1)N_{fn}(1-\sqrt{\varepsilon})^2\kappa}\right) \end{aligned} \tag{33}$$

where the approximation $1-(1-Q(x))^n \cong nQ(x)$ is used. In addition, the second term in (32) is ignored since (32) is dominated by the first term, which will be justified from Fig. 7 later. The detection-failure probability and the detection probability when the frame detection and the partition estimation are correct, which are $P_{\mathrm{df3}}(\kappa)$ and $P_s(\kappa)$, respectively, are then given as

$$\begin{aligned} P_{\mathrm{df3}}(\kappa) &= \Pr\left\{\max_q \Re\{\chi_{p_n,q}\} < \chi_{\mathrm{th}}\right\} \\ &= \left(1 - Q\left(\sqrt{\frac{2\varepsilon\gamma P(D-1)N_{fn}\kappa}{4\gamma P\kappa+1}}\right)\right)^{G-1} \\ &\quad \times Q\left(\sqrt{2\gamma P(D-1)N_{fn}(1-\sqrt{\varepsilon})^2\kappa}\right) \\ P_s(\kappa) &= 1 - P_{\mathrm{df3}}(\kappa) - P_{\mathrm{fa3}}(\kappa). \end{aligned} \tag{34}$$

Remark 1: In this paper, channel estimation is assumed to be perfect in the sequence estimation. However, when SNR is low (as in Figs. 7 and 8), the assumption is not valid, and the performance of the proposed scheme may severely degrade. In this case, (19) is modified as $\chi_{p,q} = \sum_{r=0}^{N_{fn}-1} |\sum_{d=0}^{D-1} Y_n(rN_{fs} + pD + d)\psi_{p,q}^*(rD+d)|^2$. Here, we assume that the channel is constant within D adjacent subcarriers, which is practically acceptable if D is appropriately selected.

D. Overall Cell-Identification Performance

Let $P_{\mathrm{fa,FDE}}(\kappa)$, $P_{\mathrm{df,FDE}}(\kappa)$, $P_{\mathrm{fa,FDC}}(\kappa)$, $P_{\mathrm{df,FDC}}(\kappa)$, and $P_{s,\mathrm{FDC}}(\kappa)$ denote the false-alarm probability of the cell identification when the frame detection is erroneous, the detection-failure probability of the cell identification when the frame detection is erroneous, the false-alarm probability of the cell identification when the frame detection is correct, the detection-failure probability of the cell identification when the frame detection is correct, and the detection probability of the cell identification, respectively. First, consider the overall cell-identification performance when $N_c = 1$. In this case, it is straightforward to show that

$$\begin{aligned} P_{\mathrm{fa,FDE}}(\kappa) &= P_{\mathrm{fa1}}(\kappa) \triangleq \bar{P}_{\mathrm{fa,FDE}}(\kappa) \\ P_{\mathrm{df,FDE}}(\kappa) &= P_{\mathrm{df1}}(\kappa) \triangleq \bar{P}_{\mathrm{df,FDE}}(\kappa). \end{aligned} \tag{35}$$

When the frame detection is correct, we obtain $P_{\mathrm{fa,FDC}}(\kappa)$, $P_{\mathrm{df,FDC}}(\kappa)$, and $P_{s,\mathrm{FDC}}(\kappa)$ from (26) and (31)–(34) as

$$\begin{aligned} P_{\mathrm{fa,FDC}}(\kappa) &= P_{e,\mathrm{part}}(\kappa)P_{\mathrm{fa2}}(\kappa) + (1 - P_{e,\mathrm{part}}(\kappa))\, P_{\mathrm{fa3}}(\kappa) \\ &\triangleq \bar{P}_{\mathrm{fa,FDC}}(\kappa) \\ P_{\mathrm{df,FDC}}(\kappa) &= P_{e,\mathrm{part}}(\kappa)P_{\mathrm{df2}}(\kappa) + (1 - P_{e,\mathrm{part}}(\kappa))\, P_{\mathrm{df3}}(\kappa) \\ &\triangleq \bar{P}_{\mathrm{df,FDC}}(\kappa) \\ P_{s,\mathrm{FDC}}(\kappa) &= 1 - P_{\mathrm{fa,FDC}}(\kappa) - P_{\mathrm{df,FDC}}(\kappa) \\ &= (1 - P_{e,\mathrm{part}}(\kappa))\, P_s(\kappa) \triangleq \bar{P}_{s,\mathrm{FDC}}(\kappa). \end{aligned} \tag{36}$$

The error events of the partition estimation and the sequence estimation are not independent because both estimations are based on the same OFDM symbol. However, we ignore the dependence in (36) for simplicity, which will be justified from the simulation results in Section VI. Now, consider the case where $N_c > 1$. When a frame detection error occurs, a false alarm occurs only when the sequences in all N_c symbols are falsely detected. In this case, we have

$$\begin{aligned} P_{\mathrm{fa,FDE}}(\kappa) &= \bar{P}^{N_c}_{\mathrm{fa,FDE}}(\kappa) \\ P_{\mathrm{df,FDE}}(\kappa) &= 1 - P_{\mathrm{fa,FDE}}(\kappa) = 1 - \bar{P}^{N_c}_{\mathrm{fa,FDE}}(\kappa). \end{aligned} \tag{37}$$

When the frame detection is correct, a successful detection occurs only when all N_c symbols are correctly detected. In this case, we have

$$P_{s,\mathrm{FDC}}(\kappa) = \bar{P}^{N_c}_{s,\mathrm{FDC}}(\kappa). \tag{38}$$

When a detection failure does not occur during all N_c symbols, then either a correct detection or a false alarm occurs. Thus, we have

$$P_{\mathrm{fa,FDC}}(\kappa) = \left(1 - \bar{P}_{\mathrm{df,FDC}}(\kappa)\right)^{N_c} - \bar{P}^{N_c}_{s,\mathrm{FDC}}(\kappa). \tag{39}$$

Finally, the detection failure occurs when the detection fails at least once. In this case, we have

$$P_{\mathrm{df,FDC}}(\kappa) = 1 - \left(1 - \bar{P}_{\mathrm{df,FDC}}(\kappa)\right)^{N_c}. \tag{40}$$

V. MAT Analysis

In Fig. 3, the state diagram for the proposed cell search is shown. Here, the states denoted as P, OT, and FA represent the preamble S-field, an OFDM symbol except for the preamble S-field, and the false alarm status, respectively. In addition, G_p and G_{ot} represent groups of N_h consecutive states (OFDM symbols), and N_p denotes the penalty time (in the number of OFDM symbols) due to the false alarm. For analytical purposes, we assume the following.

Assumption 1) The next state of the FA state should be the first state in the group in which the last false alarm occurred.

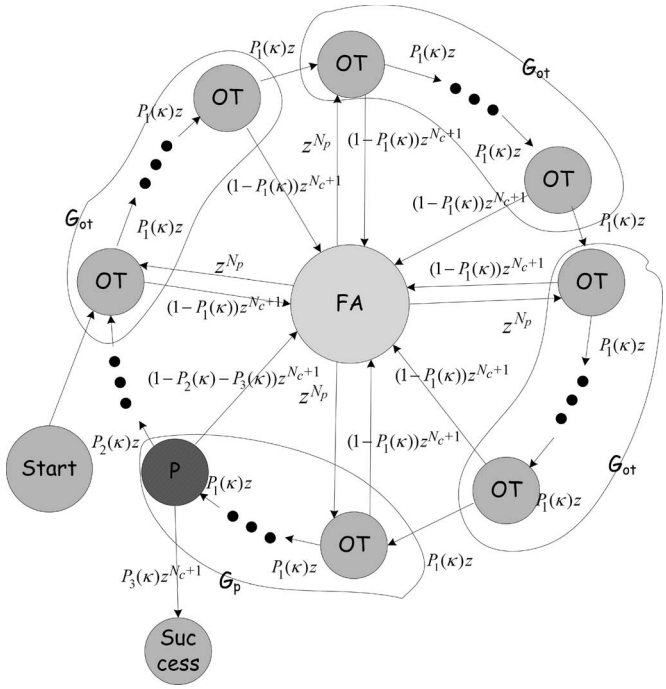

Fig. 3. State transition diagram for acquisition.

Assumption 2) The starting point of the frame detection is the first state of the group that is θ groups away from the G_p group.

Assumption 3) θ is uniformly distributed among $0, 1, \ldots, N_f/N_h - 1$, where N_f is the number of OFDM symbols in a frame.

Assumption 4) The frame detection, the fine timing estimation, and the cell-identification processes are performed in a fully pipelined structure.

In addition, define the probabilities $P_1(\kappa)$, $P_2(\kappa)$, and $P_3(\kappa)$ as follows:

1) $P_1(\kappa)$: the transition probability from an OT state to the next OT (or P) state, which is for the case that either a false frame detection does not occur or a false frame detection occurs with the failure of the cell identification;
2) $P_2(\kappa)$: the transition probability from the P state to the next OT state, which is the case that either the frame detection fails or the frame detection is successful with the failure of the cell identification;
3) $P_3(\kappa)$: the transition probability from the P state to the success state, which is the case that both the frame detection and the cell identification are successful.

Then, we obtain $P_1(\kappa)$, $P_2(\kappa)$, and $P_3(\kappa)$ from (14), (15), and (37)–(40) as

$$\begin{aligned} P_1(\kappa) &= 1 - P_{\mathrm{fa,frame}}(\kappa) + P_{\mathrm{fa,frame}}(\kappa)P_{\mathrm{df,FDE}}(\kappa) \\ &= 1 - P_{\mathrm{fa,frame}}(\kappa)P_{\mathrm{fa,FDE}}(\kappa) \\ P_2(\kappa) &= P_{\mathrm{df,frame}}(\kappa) + (1 - P_{\mathrm{df,frame}}(\kappa))\, P_{\mathrm{df,FDC}}(\kappa) \\ P_3(\kappa) &= (1 - P_{\mathrm{df,frame}}(\kappa))\, P_{s,\mathrm{FDC}}(\kappa). \end{aligned} \tag{41}$$

Finally, a transition from a state to the next state in Fig. 3 is denoted as the form of Pz^N, where P denotes the transition

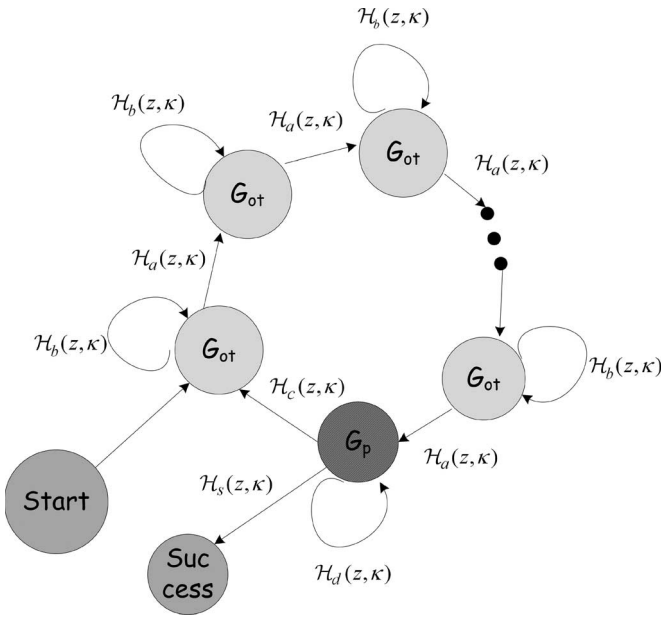

Fig. 4. Equivalent state-transition diagram for acquisition.

probability, z is a dummy variable, and N is the number of symbols required for the transition. Now, we define $\mathcal{H}(z)$ to be the transfer function of the state diagram shown in Fig. 3 between the start state and the success state. Then, it is the sum of path gains of all possible paths from the start state to the success state. Thus, the derivative of $\mathcal{H}(z)$ evaluated at $z=1$ gives the summation of the transition probability of each path multiplied by the number of symbols required for the transition along the path. This summation is the expected number of symbols required for a successful synchronization and cell search, which is referred to as the MAT [24]. To easily obtain the transfer function, we consider an equivalent state transition diagram, as shown in Fig. 4. Here, N_h consecutive states (P or OT) are represented as one state ($G_{\rm ot}$ or G_p). In addition, from assumption 1, a false alarm and its recovery can be combined to a self-transition. Let us define the transition gains $\mathcal{H}_a(z,\kappa)$, $\mathcal{H}_b(z,\kappa)$, $\mathcal{H}_c(z,\kappa)$, $\mathcal{H}_d(z,\kappa)$, and $\mathcal{H}_s(z,\kappa)$ as follows:

1) $\mathcal{H}_a(z,\kappa)$: the transition gain from a $G_{\rm ot}$ state to the next $G_{\rm ot}$ state;
2) $\mathcal{H}_b(z,\kappa)$: the self-transition gain from a $G_{\rm ot}$ state to itself;
3) $\mathcal{H}_c(z,\kappa)$: the transition gain from the G_p state to the next $G_{\rm ot}$ state;
4) $\mathcal{H}_d(z,\kappa)$: the self-transition gain from the G_p state to itself;
5) $\mathcal{H}_s(z,\kappa)$: the transition gain from the G_p state to the success state.

Then, from Fig. 3, $\mathcal{H}_a(z,\kappa)$, $\mathcal{H}_b(z,\kappa)$, $\mathcal{H}_c(z,\kappa)$, $\mathcal{H}_d(z,\kappa)$, and $\mathcal{H}_s(z,\kappa)$ are obtained as

$$\mathcal{H}_a(z,\kappa) = P_1^{N_h}(\kappa) z^{N_h}$$

$$\mathcal{H}_b(z,\kappa) = z^{N_p} \sum_{k=0}^{N_h-1} \left(1-P_1(\kappa)\right) z^{N_c+1} P_1^k(\kappa) z^k$$

$$\mathcal{H}_c(z,\kappa) = P_2(\kappa) P_1^{N_h-1}(\kappa) z^{N_h}$$

$$\mathcal{H}_d(z,\kappa) = \left(1-P_1(\kappa)\right) z^{N_p+N_c+1} \sum_{k=0}^{N_h-2} \left(P_1(\kappa) z\right)^k + P_1^{N_h-1}(\kappa)\left(1-P_2(\kappa)-P_3(\kappa)\right) z^{N_p+N_c+N_h}$$

$$\mathcal{H}_s(z,\kappa) = P_3(\kappa) P_1^{N_h-1}(\kappa) z^{N_c+N_h}. \quad (42)$$

A. Nonfading Channel

In nonfading additive white Gaussian noise (AWGN) channels, the MAT can be obtained by setting $\kappa=1$ and $N_h=1$. Define $\mathcal{H}_a(z)=\mathcal{H}_a(z,1)$, $\mathcal{H}_b(z)=\mathcal{H}_b(z,1)$, $\mathcal{H}_c(z)=\mathcal{H}_c(z,1)$, $\mathcal{H}_d(z)=\mathcal{H}_d(z,1)$, and $\mathcal{H}_s(z)=\mathcal{H}_s(z,1)$. Let $\mathcal{H}_e(z)=\mathcal{H}_a(z)/(1-\mathcal{H}_b(z))$ and $\mathcal{H}_f(z)=\mathcal{H}_c(z)/(1-\mathcal{H}_d(z))$. Then, by applying Mason's rule [23], $\mathcal{H}(z)$ is given by

$$\mathcal{H}(z) = \frac{\mathcal{H}_s(z)\mathcal{H}_e^{\theta}(z)}{1-\mathcal{H}_e^{N_f-1}(z)\mathcal{H}_f(z)}. \quad (43)$$

The MAT conditioned on θ, $\tau_{\rm MA}(\theta)=(d/dz)\mathcal{H}(z)|_{z=1}$ is given as

$$\tau_{\rm MA}(\theta) = \frac{d}{dz}\mathcal{H}(z)|_{z=1} = \frac{\mathcal{H}_s'(1)+(\theta)\mathcal{H}_s(1)\mathcal{H}_e'(1)}{1-\mathcal{H}_f(1)} + \frac{\mathcal{H}_s(1)\left((N_f-1)\mathcal{H}_e'(1)\mathcal{H}_f(1)+\mathcal{H}_f'(1)\right)}{\left(1-\mathcal{H}_f(1)\right)^2} \quad (44)$$

where $\mathcal{H}_e(1)=\mathcal{H}_a(1)/(1-\mathcal{H}_b(1))=P_1/(1-(1-P_1))=1$ is used. Since $E\{\theta\}=(N_f-1)/2$, the MAT $\tau_{\rm MA}$ is given as

$$\tau_{\rm MA} = \frac{2\mathcal{H}_s'(1)+(N_f-1)\mathcal{H}_s(1)\mathcal{H}_e'(1)}{2\left(1-\mathcal{H}_f(1)\right)} + \frac{\mathcal{H}_s(1)\left((N_f-1)\mathcal{H}_e'(1)\mathcal{H}_f(1)+\mathcal{H}_f'(1)\right)}{\left(1-\mathcal{H}_f(1)\right)^2}. \quad (45)$$

B. Fading Channel

The channel gain of each path in a fading channel is assumed to be constant during N_h symbols and independent from one N_h symbol block to another. Here, we can set $N_h \propto 1/f_d T_s$, where f_d is the maximum Doppler frequency. Define $\mathcal{H}_a(z)=E\{\mathcal{H}_a(z,\kappa)\}$, $\mathcal{H}_b(z)=E\{\mathcal{H}_b(z,\kappa)\}$, $\mathcal{H}_c(z)=E\{\mathcal{H}_c(z,\kappa)\}$, $\mathcal{H}_d(z)=E\{\mathcal{H}_d(z,\kappa)\}$, and $\mathcal{H}_s(z)=E\{\mathcal{H}_s(z,\kappa)\}$, which can be evaluated using a numerical integration. Then, $\mathcal{H}(z)$ is given by

$$\mathcal{H}(z) = \frac{\mathcal{H}_s(z)\mathcal{H}_e^{\theta}(z)}{1-\mathcal{H}_e^{N_f/N_h-1}(z)\mathcal{H}_f(z)}. \quad (46)$$

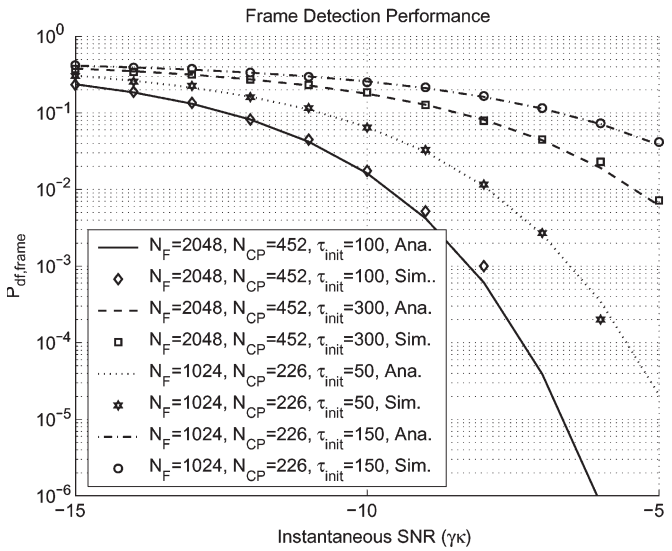

Fig. 5. Performance of the proposed frame-detection algorithm.

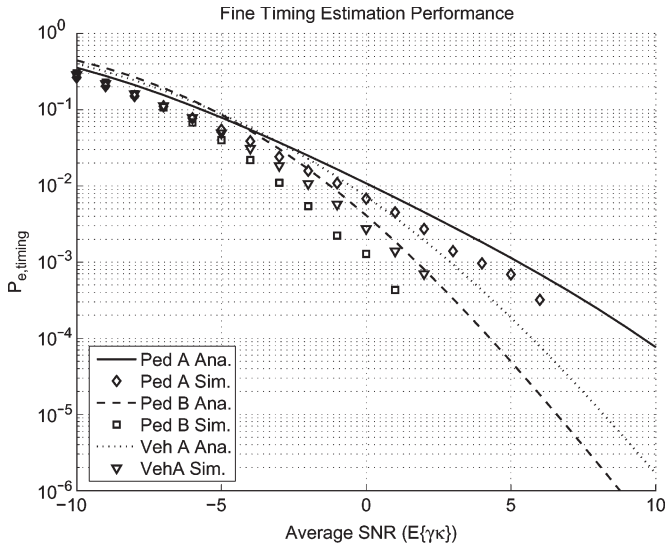

Fig. 6. Performance of the proposed fine timing-estimation algorithm.

In addition, in this case, we have $E\{\theta\} = (N_h/N_f)\sum_{k=0}^{N_f/N_h-1} k = (N_f/N_h - 1)/2$. In a similar way to (44) and (45), we can obtain

$$\tau_{\mathrm{MA}} = \frac{2\mathcal{H}_s'(1) + (N_f/N_h - 1)\,\mathcal{H}_s(1)\mathcal{H}_e'(1)}{2\left(1 - \mathcal{H}_f(1)\right)} + \frac{\mathcal{H}_s(1)\left((N_f/N_h - 1)\,\mathcal{H}_e'(1)\mathcal{H}_f(1) + \mathcal{H}_f'(1)\right)}{\left(1 - \mathcal{H}_f(1)\right)^2}. \quad (47)$$

VI. Numerical and Simulation Results

In Fig. 5, the performance of the proposed frame-detection algorithm in an AWGN channel is shown. Here, the following parameters are used: $N_F = 1024(2048)$, $N_{\mathrm{CP}} = 226(452)$, and $\tau_{\mathrm{init}} = 50(100)$ or $150(300)$ (i.e., the initial timing error is introduced without performing the initial timing estimation). In this figure, "Ana." and "Sim." stand for the analytic result obtained by (14) [or (15)] and the Monte Carlo simulation result over 100 000 runs, respectively. From Fig. 5, we can see that the derived detection-failure probability (or false-alarm probability since they are equal) is quite well matched with that from the simulation. In addition, we can see that, as N_{CP} increases, the performance of the frame detection is improved. When the initial timing-estimation error τ_{init} becomes comparable to N_{CP}, the performance of the frame detection degrades significantly due to the SNR loss [small $g = q^2(\tau_{\mathrm{init}})N_{\mathrm{CP}}$ in (15)]. However, we can improve the initial timing-estimation performance by increasing the number of symbols used in the initial timing estimation (N_{init}) in (6). When τ_{init} is small, the false-alarm probability (or the detection-failure probability) of the proposed frame detection is less than 10^{-4} at the instantaneous SNR $(\gamma\kappa)$ of -5 dB.

In Fig. 6, the performance of the proposed fine timing-estimation algorithm is shown for three different channels: the Ped. (Pedestrian) A channel, the Ped. B channel, and the Vehic. (Vehicular) A channel. Here, the following parameters

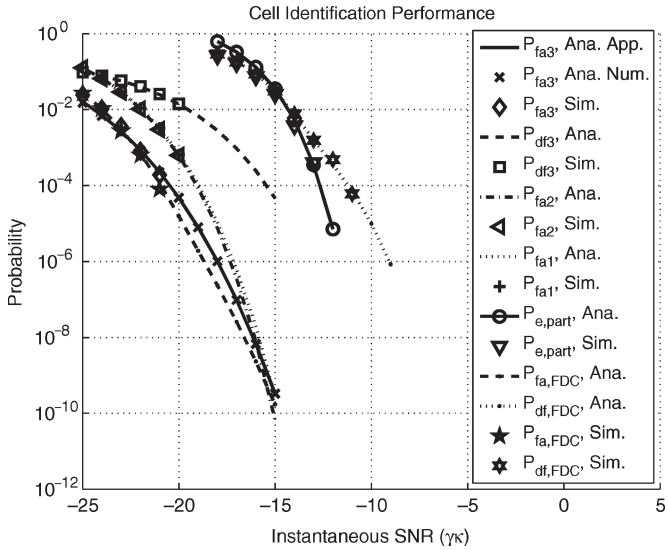

Fig. 7. Performance of the proposed cell-identification algorithm.

are commonly used: $N_F = 2048$, $R = 128$, $N_B = 60$, and $N_w = 300$. From Fig. 6, we can see that the error probabilities of the fine timing estimation obtained from (17) are slightly higher than those obtained by the Monte Carlo simulation over 10 000 runs. This is due to the approximation made in (17), where the maximum value of the magnitude of the cross correlation [$|\zeta(k)|$ in (17)] is approximated to the magnitude of the cross correlation at the point where the strongest path arrives. In [25], similar results were shown in the context of selection diversity. In addition, we can see from this figure that the performance of the proposed fine timing estimation is improved as the diversity order of the channel increases. (There exist four paths in the Ped. A channel and six paths in the Ped. B channel and Vehic. A channel. The variance of the path gains in the Ped. B channel is smaller than that in the Vehic. A channel.)

In Fig. 7, the performance of the proposed cell-identification algorithm in an AWGN channel is shown. In this figure, "Ana.," "Ana. Num.," and "Sim." stand for the analytic result

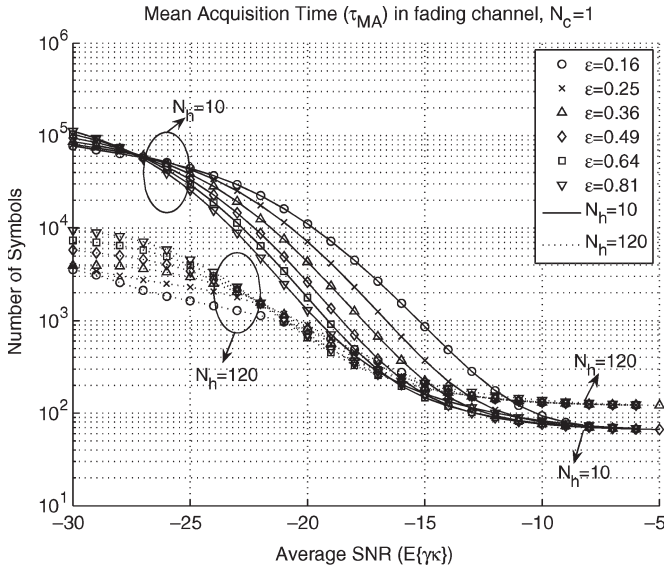

Fig. 8. MAT in Vehicular A fading channel.

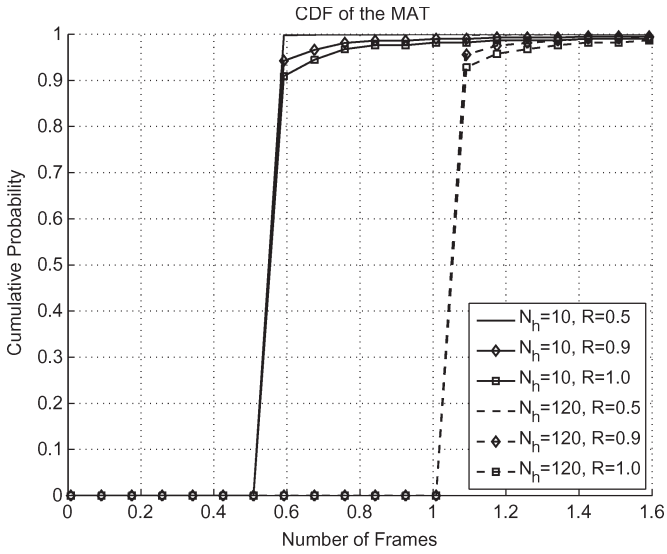

Fig. 9. CDF of the MAT in multicell environments.

obtained by (26), (30), (31), (33), (34), and (36), the analytic result obtained by (32) using numerical integration, and the Monte Carlo simulation result over 100 000 runs, respectively. Here, the following parameters are used: $N_F = 2048$, $P = 8$, $G = 8$, $D = 8$, and $\varepsilon = 0.6$. It is shown that, from Fig. 7, the derived false-alarm probabilities, the detection-failure probabilities, and the partition-error probability are quite well matched with those from the Monte Carlo simulation over 100 000 runs. In addition, one can see that the false-alarm probabilities, the detection-failure probability, and the partition-error probability are lower than 10^{-4} at the instantaneous SNR $(\gamma\kappa)$ of -12 dB or less.

In Fig. 8, the MAT in the Vehic. A fading channel is shown for various values of N_h and ε, when $N_F = 2048$, $N_{\mathrm{CP}} = 452$, $\tau_{\mathrm{init}} = 100$, $P = 8$, $G = 8$, $D = 8$, $N_f = 120$, $N_p = 1200$, and $N_c = 1$. When SNR is low, the MAT increases as N_h decreases (the mobile speed increases). This can be explained as follows. Since SNR is low, the threshold for the sequence estimation becomes low, and the false alarm is likely to occur. As the mobile speed increases, the instantaneous SNR and the corresponding threshold fluctuate within a frame. Thus, the probability that the threshold remains above the noise level during a frame decreases, and the false alarm is more likely to occur. However, as SNR increases, the MATs decrease down to 67 and 122 symbols when $N_h = 10$ (for a fast mobile speed) and $N_h = 120$ (for a slow mobile speed), respectively, at the average SNR of -5 dB. From Fig. 8, one can see that a good choice for $\sqrt{\varepsilon}$ lies between 0.7 and 0.8.

Since the common preamble S-field is used for all base stations, the received preamble S-field signal in a multicell environment is identical to that in the single-cell case with an enlarged delay spread. Thus, little changes in the initial timing synchronization and the frame detection in multicell environments. For the cell identification, neighboring cells do not interfere with each other since they use different partitions in the preamble C-field. Thus, if the intercell interference from neighboring cells are only taken into account, the cell-identification performance in multicell environment is the same with that in the single-cell case. In Fig. 9, the cumulative distribution function (CDF) of the MAT at the center cell in the multicell environment with 49 hexagonal cells (seven clusters, seven hexagonal cells per cluster), which is numerically obtained using the result in Fig. 8, is shown. Here, the normalized distance R denotes the distance between the nearest base station and the mobile station divided by the cell radius. In addition, the path-loss decay factor, the log-normal shadowing standard deviation, the shadowing correlation between cells, and the signal-to-background-noise ratio at the cell boundary without shadowing variation are set at 4.0, 8 dB, 0.5, and 3 dB, respectively. It is shown that the MAT is less than two frames with the probability very close to one even at cell boundary, which shows the reliable performance of the proposed scheme.

Although a detailed performance–complexity comparison between the proposed scheme and that in [7] or the IEEE802.16e [10] is beyond the scope of this paper, a brief qualitative discussion on the obvious advantages of the proposed scheme can be summarized as follows.

1) Advantages over that in [7] are as follows.
   a) A fine timing synchronization is available using the preamble S-field.
   b) The integral part of the frequency offset, as well as the fractional part of the frequency offset, can be estimated due to the preamble S-field.
   c) Low intercell interference in the cell-identification process is obtained since the orthogonality between different subcarriers in the preamble C-field is much better than that between different pseudonoise codes in CPICH.
2) The advantages over the IEEE802.16e default mode (without the optional preamble) are as follows.
   a) For timing-estimation complexity, the number of candidates in the proposed scheme is $N_s(\text{initial timing}) + N_f(\text{frame timing}) + N_w$ (fine timing), while that of IEEE802.16e using the algorithm in [16] is $N_s N_f$.

b) The estimation of the integral part of the frequency offset and the cell identification should be jointly performed in IEEE802.16e, which greatly increases the cell-identification complexity.

3) The advantages over IEEE802.16e optional mode (with the optional preamble) are as follows.
   a) The frame-timing estimation is easier due to the unique postfix structure of the preamble S-field.
   b) A partition comprised of consecutive comb sets can reduce the interference from neighboring cells when the frequency offset between base stations exists.
   c) The cell-identification performance can be improved using coherent combining.

Remark 2: Consider the performance of the proposed scheme when the approach in Remark 1 is applied. In Figs. 7 and 8, $N_F = 2048$, $P = 8$, and $D = 8$ are used. Let the instantaneous SNR be -17 dB. Then, the symbol SNR at a subcarrier in s_{p_n} is -8 dB (P times boosted). If channel estimation is perfect, and $N_F/P = 256$ symbols are coherently combined as in (19), the combined SNR becomes 16 dB. The noncoherent combining loss when the coherently combined SNR is 16 dB and the number of branches for the noncoherent combining is $N_F/P/D = 32$ is about 3 dB (see [22, Fig. 12.1-1]). Similarly, when the instantaneous SNR is -25 dB, the noncoherent combining loss is about 5 dB. Now, let the average SNR (the x-axis in Fig. 8) be -15 dB. Since the probability that instantaneous SNR is below -10 dB of the average SNR in the Vehicular A channel is quite low (say, below 10^{-4}), we can say that the performance degradation is less than 5 dB, and the proposed scheme provides robust cell-search performance when the average SNR is as low as -10 dB in practice.

VII. Concluding Remark

In this paper, a novel preamble-based synchronization and cell-search technique for OFDM cellular systems was proposed. The preamble is composed of the S-field and the C-field, and the corresponding synchronization and cell-search algorithm is constructed in a hierarchical approach for both the synchronization and the cell search. The synchronization algorithm includes the initial symbol-timing estimation, the initial frequency-offset estimation, the frame detection, the fine symbol-timing estimation, and the frequency-offset estimation. The cell-search algorithm is proceeded in a hierarchical manner, including the partition estimation and the sequence estimation on each symbol of the preamble C-field. The performance of each synchronization and cell-search step was analyzed, and the overall performance of the synchronization and cell search was analyzed in terms of MAT in AWGN- and frequency-selective fading channels. Computer simulations were performed to verify the analytic results derived in this paper.

From the numerical results, it was shown that the performance of the proposed frame-detection algorithm degrades as the length of the guard interval decreases. In addition, the performance of the fine timing estimation is improved as the frequency diversity of the channel increases as long as the back-off time is larger than the maximum nonnegligible delay spread. In addition, it was shown that the MAT increases as the mobile speed gets slower in a fading channel. However, at the average SNR of -5 dB, the MAT is just slightly higher than the frame length. As the mobile speed increases, the MAT decreases, except for the case of a very low average SNR (say, less than -10 dB). Furthermore, from the CDF of the MAT, it was seen that at most two frames are required for a successful cell search in multicell environments. Therefore, we can conclude that the proposed preamble and the corresponding algorithm provide very robust synchronization and cell-search capability, even in bad cellular environments.

Appendix A
Derivation of the Statistics of $z(k)$ and $\zeta(k)$

Assuming that the transmitted symbol is not the preamble S-field, the transmitted signal $x(k)$ can be represented as

$$x(k) = \begin{cases} \frac{1}{\sqrt{N_F}} \sum_{p=0}^{N_F-1} X_a(p) \\ \quad \times \exp\left(-\frac{j2\pi p(k-N_{\mathrm{CP}})}{N_F}\right), & N_{\mathrm{CP}} \le b < N_s \\ x(k+N_s-N_{\mathrm{CP}}), & 0 \le b < N_{\mathrm{CP}} \end{cases} \tag{A1}$$

where $k = aN_s + b$, and $0 \le b < N_s$. Here, we assume that $\{X_a(p)\}$ is a zero-mean i.i.d. random process. Then, for sufficiently large N_F, we can assume that $x(k)$ is a Gaussian random process with $E\{x(k)\} = 0$ and that

$$\begin{aligned} &E\{x^*(k)x(n)\} \\ &= \frac{1}{N_F} \sum_{p=0}^{N_F-1} \sum_{q=0}^{N_F-1} E\{X_a^*(p)X_c(q)\} \exp\left(-\frac{j2\pi(pk'-qn')}{N_F}\right) \\ &= \frac{\delta_{\mathrm{K}}(a-c)}{N_F} \sum_{p=0}^{N_F-1} E\left\{|X_a(p)|^2\right\} \exp\left(-\frac{j2\pi p(k'-n')}{N_F}\right) \\ &= \frac{P_x}{N_F}\delta_{\mathrm{K}}(a-c)(\delta_{\mathrm{K}}(k-n)+\delta_{\mathrm{K}}(k-n\pm N_F)) \end{aligned} \tag{A2}$$

where $n = cN_s + d$, $0 \le d < N_s$, $k' = k - N_{\mathrm{CP}}$, $n' = n - N_{\mathrm{CP}}$, and $P_x = \sum_{p=0}^{N_F-1} E\{|X(p)|^2\}$. The second and the third equalities of (A2) come from the fact that $E\{X_a^*(p)X_c(q)\} = 0$ for $p \ne q$ or $a \ne c$ due to the independence of the transmitted symbols and that the summation becomes zero, except in the case where $k' - n' = k - n$ is a multiple of N_F, respectively. After some mathematical manipulation on (5), we have

$$\begin{aligned} z(k) = &\sum_{l_1=0}^{L-1} \sum_{l_2=0}^{L-1} h_{l_1}^* h_{l_2} r_x(k-\tau_{l_1}, \tau_{l_1}-\tau_{l_2}) \\ &+ \sum_{l=0}^{L-1} h_l^* \mu(k-\tau_l, N_F+\tau_l) \\ &+ \sum_{l=0}^{L-1} h_l \mu^*(k+N_F-\tau_l, \tau_l-N_F) + \eta(k) \end{aligned} \tag{A3}$$

where $r_x(k,\alpha) = (1/N_{\mathrm{CP}}) \sum_{r=0}^{N_{\mathrm{CP}}-1} x^*(k+r)x(k+r+N_F+\alpha)$, $\mu(k,\alpha) = (1/N_{\mathrm{CP}}) \sum_{r=0}^{N_{\mathrm{CP}}-1} x^*(k+r)n(k+r+\alpha)$, and $\eta(k) = (1/N_{\mathrm{CP}}) \sum_{r=0}^{N_{\mathrm{CP}}-1} n^*(k+r)n(k+r+N_F)$. Then, we

have $E\{\mu(k,\alpha)\}=0$ and $E\{\eta(k)\}=0$. Furthermore, from (A2), we have

$$E\{r_x(k,\alpha)\}=\frac{1}{N_{\mathrm{CP}}}\sum_{r=0}^{N_{\mathrm{CP}}-1}E\{x^*(k+r)x(k+r+N_F+\alpha)\}=\frac{P_x}{N_F}q(k)\delta_{\mathrm{K}}(\alpha). \tag{A4}$$

In addition, it is easily seen that

$$\begin{aligned}&\mathrm{Var}\{\mu(k,\alpha)\}\\&=\frac{1}{N_{\mathrm{CP}}^2}\sum_{r_1=0}^{N_{\mathrm{CP}}-1}\sum_{r_2=0}^{N_{\mathrm{CP}}-1}E\{x^*(k+r_1)\}x\{(k+r_2)\}\\&\quad\times E\{n(k+r_1+\alpha)n^*(k+r_2+\alpha)\}\\&=\frac{1}{N_{\mathrm{CP}}^2}\sum_{r=0}^{N_{\mathrm{CP}}-1}E\left\{|x(k+r)|^2\right\}E\left\{|n(k+r+\alpha)|^2\right\}\\&=\frac{2P_x\sigma_n^2}{N_{\mathrm{CP}}N_F}\end{aligned} \tag{A5}$$

and

$$\begin{aligned}&\mathrm{Var}\{\eta(k)\}\\&=\frac{1}{N_{\mathrm{CP}}^2}\sum_{r_1=0}^{N_{\mathrm{CP}}-1}\sum_{r_2=0}^{N_{\mathrm{CP}}-1}E\{n^*(k+r_1)n(k+r_2)\\&\qquad\times n(k+r_1+N_F)n^*(k+r_2+N_F)\}\\&=\frac{1}{N_{\mathrm{CP}}^2}\sum_{r=0}^{N_{\mathrm{CP}}-1}E\left\{|n(k+r)|^2\right\}E\left\{|n(k+r+N_F)|^2\right\}\\&=\frac{4\sigma_n^4}{N_{\mathrm{CP}}}.\end{aligned} \tag{A6}$$

Therefore, for sufficiently large N_{CP}, we can assume by the CLT that $z(k)$ is a Gaussian process with the following mean $m_z(k)$ and variance $2\sigma_z^2(k)$:

$$\begin{aligned}m_z(k)&=\sum_{l_1=0}^{L-1}\sum_{l_2=0}^{L-1}h_{l_1}^*h_{l_2}E\{r_x(k-\tau_{l_1},\tau_{l_1}-\tau_{l_2})\}\\&=\frac{P_x}{N_F}\sum_{l=0}^{L-1}|h_l|^2q(k-\tau_l)\\&\cong\frac{P_xq(k)\kappa}{N_F}\end{aligned} \tag{A7}$$

and

$$\begin{aligned}\sigma_z^2(k)&=\frac{1}{2}\sum_{l_1=0}^{L-1}\sum_{l_2=0}^{L-1}|h_{l_1}|^2|h_{l_2}|^2\,\mathrm{Var}\{r_x(k-\tau_{l_1},\tau_{l_1}-\tau_{l_2})\}\\&\quad+\frac{1}{2}\sum_{l=0}^{L-1}|h_l|^2\left(\mathrm{Var}\{\mu(k-\tau_l,N_F+\tau_l)\}\right.\\&\qquad\left.+\mathrm{Var}\{\mu^*(k+N_F-\tau_l,\tau_l-N_F)\}\right)\\&\quad+\frac{1}{2}\mathrm{Var}\{\eta(k)\}\\&\cong\frac{2\sigma_n^2P_x\kappa}{N_{\mathrm{CP}}N_F}+\frac{2\sigma_n^4}{N_{\mathrm{CP}}}.\end{aligned} \tag{A8}$$

The approximation in (A7) comes from the fact that $\sum_{l=0}^{L-1}q(k-\tau_l)|h_l|^2\cong q(k)\kappa$ since $q(k-\tau_l)=\max(0,1-|k-\tau_l|/N_{\mathrm{CP}})\cong q(k)$ when $\tau_l\ll N_{\mathrm{CP}}$ and $|h_l|^2\ll 1$ with high probability when τ_l is comparable to N_{CP}. In addition, the approximation in (A8) comes from the fact that the interested range of $P_x/2\sigma_n^2N_F$ is much less than one so that the first term in (A8) can be ignored. If the transmitted symbol is the preamble S-field, we have $E\{x^*(k)x(n)\}=(P_x/N_F)\delta_{\mathrm{K}}(a-c)(\delta_{\mathrm{K}}(k-n)-\delta_{\mathrm{K}}(k-n\pm N_F))$. Thus, we have $m_z(k)\cong-(P_xq(k)\kappa/N_F)$, while $\sigma_z^2(k)$ is unchanged.

From (12), we have

$$\zeta(k)=\sum_{l=0}^{L-1}h_lc_x(k-\tau_l)+n_c(k) \tag{A9}$$

where $c_x(k)=(1/R)\sum_{r=0}^{R-1}x^*(r+R_s)x(k+r+R_s)$, and $n_c(k)=(1/R)\sum_{r=0}^{R-1}x^*(r+R_s)n(k+r+R_s)$. Following a similar procedure, we obtain

$$E\{c_x(k)\}=\frac{1}{R}\sum_{r=0}^{R-1}E\{x^*(r+R_s)x(k+r+R_s)\}=\frac{P_x}{N_F}\delta_{\mathrm{K}}(k) \tag{A10}$$

$$\begin{aligned}E\{c_x^*(k)c_x(n)\}&=\frac{1}{R^2}\sum_{r_1=0}^{R-1}\sum_{r_2=0}^{R-1}\\&\quad\times E\{x(r_1+R_s)x^*(k+r_1+R_s)\\&\qquad\times x^*(r_2+R_s)x(n+r_2+R_s)\}\\&=\begin{cases}\frac{P_x^2}{RN_F^2}, & k=n\neq 0\\ \frac{P_x^2}{N_F^2}, & k=n=0\\ 0, & \text{otherwise}\end{cases}\end{aligned} \tag{A11}$$

$$E\{n_c(k)\}=\frac{1}{R}\sum_{r=0}^{R-1}E\{x^*(r+R_s)n(k+r+R_s)\}=0 \tag{A12}$$

and

$$\begin{aligned}E\{n_c^*(k)n_c(m)\}&=\frac{1}{R^2}\sum_{r_1=0}^{R-1}\sum_{r_2=0}^{R-1}\\&\quad\times E\{x(r_1+R_s)n^*(k+r_1+R_s)\\&\qquad\times x^*(r_2+R_s)n(m+r_2+R_s)\}\\&=\frac{1}{R^2}\sum_{r_1=0}^{R-1}\sum_{r_2=0}^{R-1}E\{x(r_1+R_s)x^*(r_2+R_s)\}\\&\quad\times E\{n^*(k+r_1+R_s)n(m+r_2+R_s)\}\\&=\frac{2\sigma_n^2P_x}{RN_F}\delta_{\mathrm{K}}(k-m).\end{aligned} \tag{A13}$$

Therefore, we can conclude that $\zeta(k)$ is a complex Gaussian random process with mean $m_\zeta(k)$ and variance $2\sigma_\zeta^2(k)$, where

$$\begin{aligned} m_\zeta(k) &= E\{\zeta(k)\} \\ &= \sum_{l=0}^{L-1} h_l E\{c_x(k-\tau_l)\} + E\{n_c(k)\} \\ &= \frac{P_x}{N_F}\sum_{l=0}^{L-1} h_l \delta_{\mathrm{K}}(k-\tau_l) \end{aligned} \tag{A14}$$

and

$$\begin{aligned} 2\sigma_\zeta^2(k) &= \mathrm{Var}\{\zeta(k)\} \\ &= \sum_{l_1=0}^{L-1}\sum_{l_2=0}^{L-1} h_{l_1}^* h_{l_2} E\{c_x^*(k-\tau_{l_1})c_x(k-\tau_{l_2})\} \\ &\quad - m_\zeta^2(k) + \mathrm{Var}\{n_c(k)\} \\ &= \sum_{l=0}^{L-1} |h_l|^2 E\left\{|c_x(k-\tau_l)|^2\right\} \\ &\quad - \frac{P_x^2}{N_F^2}\sum_{l=0}^{L-1}|h_l|^2\delta_{\mathrm{K}}(k-\tau_l) + \frac{2\sigma_n^2 P_x}{RN_F} \\ &= \frac{P_x^2}{RN_F^2}\sum_{l=0}^{L-1}|h_l|^2\left(1-\delta_{\mathrm{K}}(k-\tau_l)\right) + \frac{2\sigma_n^2 P_x}{RN_F} \\ &\cong \frac{P_x^2\kappa}{RN_F^2} + \frac{2\sigma_n^2 P_x}{RN_F}. \end{aligned} \tag{A15}$$

APPENDIX B
DERIVATION OF (17)

Since we assume that $|\zeta(k)|^2$, $k \in K_f$, is an independent and identical chi-square random process, the conditional error probability $P_e(\nu)$ on $\nu = \max_{0\le l<L(N_B)}|h_l|^2$ is given by [22]

$$\begin{aligned} P_e(\nu) &\cong \Pr\left\{|\zeta(\tau_l)|^2 < \max_{k\in K_f}|\zeta(k)|^2 \,|\, l = \arg\max_{0\le l<L(N_B)}|h_l|\right\} \\ &= \sum_{m=1}^{N_w-N_B}(-1)^{m+1}\binom{N_w-N_B}{m}\frac{1}{m+1}\exp\left(-\frac{mR\gamma\nu}{m+1}\right). \end{aligned} \tag{B1}$$

Since $|h_l|^2$, $l=0,\ldots,L(N_B)-1$ are independent and exponentially distributed random variables with mean β_l, the cdf of ν is given by

$$\begin{aligned} F_\nu(x) &= \Pr\left\{|h_0|^2 < x, \ldots, \left|h_{L(N_B)-1}\right|^2 < x\right\} \\ &= \prod_{i=0}^{L(N_B)-1}\left(1-\exp\left(\frac{-x}{\beta_i}\right)\right) \\ &= \sum_{n=0}^{L(N_B)}\sum_{v\in V_n}(-1)^n\exp(-v^T w x). \end{aligned} \tag{B2}$$

By taking the derivative of (B2) with respect to x, the probability density function of ν is given by

$$f_\nu(x) = \sum_{l=0}^{L(N_B)-1}\prod_{i=0,i\ne l}^{L(N_B)-1}\frac{1}{\beta_l}\left(1-\exp(-x/\beta_i)\right)\exp(-x/\beta_l). \tag{B3}$$

Thus, we obtain

$$\begin{aligned} &E\left\{\exp\left(-\frac{mR\gamma}{m+1}x\right)\right\} \\ &= \int_0^\infty \exp\left(-\frac{mR\gamma}{m+1}x\right) f_\nu(x)dx \\ &= \frac{mR\gamma}{(m+1)}\int_0^\infty \exp\left(-\frac{mR\gamma}{m+1}x\right) F_\nu(x)dx \\ &= \frac{mR\gamma}{(m+1)}\sum_{n=0}^{L(N_B)}\sum_{v\in V_n}(-1)^n \\ &\quad \times \int_0^\infty \exp\left(-\left(\frac{mR\gamma}{m+1}+v^T w\right)x\right)dx \\ &= (m+1)\sum_{n=1}^{L(N_B)}\sum_{v\in V_n}(-1)^{n+1}\frac{v^T w(R\gamma+v^T w)^{-1}}{m+v^T w(R\gamma+v^T w)^{-1}}. \end{aligned} \tag{B4}$$

Using (B1) and (B4), we obtain the timing-error probability as

$$\begin{aligned} P_e &= E\{P_e(\nu)\} \\ &\cong \sum_{m=1}^{N_w-N_B}(-1)^{m+1}\binom{N_w-N_B}{m}\frac{1}{m+1} \\ &\quad \times E\left\{\exp\left(-\frac{mR\gamma\nu}{m+1}\right)\right\} \\ &= \sum_{n=1}^{L(N_B)}\sum_{v\in V_n}(-1)^{n+1}\sum_{m=1}^{N_w-N_B}(-1)^{m+1}\binom{N_w-N_B}{m} \\ &\quad \times \frac{v^T w(R\gamma+v^T w)^{-1}}{m+v^T w(R\gamma+v^T w)^{-1}} \\ &= \sum_{n=1}^{L(N_B)}\sum_{v\in V_n}(-1)^{n+1} \\ &\quad \times \left(1-\frac{v^T w}{R\gamma+v^T w}B\left(N_w-N_B+1,\frac{v^T w}{R\gamma+v^T w}\right)\right) \\ &= 1-\sum_{n=1}^{L(N_B)}\sum_{v\in V_n}(-1)^{n+1}\frac{v^T w}{R\gamma+v^T w} \\ &\quad \times B\left(N_w-N_B+1,\frac{v^T w}{R\gamma+v^T w}\right) \end{aligned} \tag{B5}$$

where $B(M,v)$ is the beta function, and the third equality comes from the fact that

$$\begin{aligned} B(M,v) &= \int_0^1 x^{v-1}(1-x)^{M-1}dx \\ &= \int_0^1 \sum_{n=0}^{M-1} \binom{M-1}{n}(-1)^n x^{n+v-1}dx \\ &= \sum_{n=0}^{M-1}(-1)^n \binom{M-1}{n}\frac{1}{n+v} \end{aligned} \tag{B6}$$

and the last equality comes from the fact that $\sum_{n=1}^{L(N_B)}\sum_{v\in V_n}(-1)^{n+1} = \sum_{n=1}^{L(N_B)}(-1)^{n+1}\binom{L(N_B)}{n} = 1 - \sum_{n=0}^{L(N_B)}(-1)^n\binom{L(N_B)}{n} = 1$.

Appendix C
Derivation of (27) and (28)

When $p = p_n$, we have

$$\begin{aligned} \chi_{p_n,q} &= \sum_{j=0}^{J_{p_n}-1} Y_n\left(s_{p_n,c}(j)\right)\hat{H}^*\left(s_{p_n,c}(j)\right)\psi^*_{p_n,q}(j) \\ &= \sqrt{\frac{P_xP}{N_F}}\sum_{d=0}^{D-2}\sum_{r=0}^{N_{fn}-1} Y_n\left(rN_{fs}+p_nD+d'\right) \\ &\quad\times H^*\left(rN_{fs}+p_nD+d'\right)\psi^*_{p_n,q}\left(r(D-1)+d\right) \\ &= \frac{P_xP}{N_F}\sum_{d=0}^{D-2}\sum_{r=0}^{N_{fn}-1}\left|H\left(rN_{fs}+p_nD+d'\right)\right|^2 \\ &\quad\times \psi_{p_n,q_n}\left(r(D-1)+d\right)\psi^*_{p_n,q}\left(r(D-1)+d\right) \\ &\quad+\sqrt{\frac{P_xP}{N_F}}\sum_{d=0}^{D-2}\sum_{r=0}^{N_{fn}-1} N\left(rN_{fs}+p_nD+d'\right) \\ &\quad\times H^*\left(rN_{fs}+p_nD+d'\right)\psi^*_{p_n,q}\left(r(D-1)+d\right) \end{aligned} \tag{C1}$$

where $d' = d$ for $d < \lfloor D/2\rfloor$, and $d' = d+1$, otherwise. If $q = q_n$, (C1) can be further simplified as

$$\begin{aligned} \chi_{p_n,q_n} &= \frac{P_xP}{N_F}\sum_{d=0}^{D-2}\sum_{r=0}^{N_{fn}-1}\left|H\left(rN_{fs}+p_nD+d'\right)\right|^2 \\ &\quad+\sqrt{\frac{P_xP}{N_F}}\sum_{d=0}^{D-2}\sum_{r=0}^{N_{fn}-1} N\left(rN_{fs}+p_nD+d'\right) \\ &\quad\times H^*\left(rN_{fs}+p_nD+d'\right)\psi^*_{p_n,q_n}\left(r(D-1)+d\right) \\ &= \frac{P_xP}{N_F}(D-1)N_{fn}\kappa + n_{\chi_{p_n,q_n}} \end{aligned} \tag{C2}$$

where $E\{n_{\chi_{p_n,q_n}}\} = 0$, and

$$\begin{aligned} \mathrm{Var}\{n_{\chi_{p_n,q_n}}\} &= \frac{2P_xP\sigma_n^2}{N_F}\sum_{d=0}^{D-2}\sum_{r=0}^{N_{fn}-1}\left|H\left(rN_{fs}+p_nD+d'\right)\right. \\ &\qquad\left.\times\,\psi_{p_n,q_n}(r(D-1)+d)\right|^2 \\ &= \frac{2P_xP\sigma_n^2(D-1)N_{fn}\kappa}{N_F}. \end{aligned} \tag{C3}$$

Thus, χ_{p_n,q_n} is a Gaussian random variable with mean $(P_xP/N_F)(D-1)N_{fn}\kappa$ and variance $(2P_xP\sigma_n^2/N_F)(D-1)N_{fn}\kappa$. If $q \neq q_n$, (C1) can be expressed as

$$\begin{aligned} \chi_{p_n,q} &= \frac{P_xP}{N_F}\sum_{d=0}^{D-2}\sum_{r=0}^{N_{fn}-1}\left|H\left(rN_{fs}+p_nD+d'\right)\right|^2 \\ &\quad\times\psi_{p_n,q_n}\left(r(D-1)+d\right) \\ &\quad\times\psi^*_{p_n,q}\left(r(D-1)+d\right)+n_{\chi_{p_n,q}} \\ &= i_{\chi_{p_n,q}} + n_{\chi_{p_n,q}} \end{aligned} \tag{C4}$$

where $i_{\chi_{p_n,q}}$ is approximated as a Gaussian random variable by CLT with $E\{i_{\chi_{p_n,q}}\} = 0$ and (C5), shown at the bottom of the page. Here, we assume that $\tau_{l_1} - \tau_{l_2} + \tau_{l_3} - \tau_{l_4} = 0$ only when either $\tau_1 = \tau_2$ and $\tau_3 = \tau_4$, or $\tau_1 = \tau_4$ and $\tau_2 = \tau_3$ in deriving (C5). Thus, considering the worst case, $\chi_{p_n,q}$, $q \neq q_n$ is approximated as a Gaussian random variable with

$$\begin{aligned} \mathrm{Var}\{i_{\chi_{p_n,q}}\} &= \frac{P_x^2P^2}{N_F^2}\sum_{d=0}^{D-2}\sum_{r=0}^{N_{fn}-1}\left|H\left(rN_{fs}+p_nD+d'\right)\right|^4 \\ &= \frac{P_x^2P^2}{N_F^2}\sum_{d=0}^{D-2}\sum_{l_1=0}^{L-1}\sum_{l_2=0}^{L-1}\sum_{l_3=0}^{L-1}\sum_{l_4=0}^{L-1} h^*_{l_1}h_{l_2}h^*_{l_3}h_{l_4}\exp\left(-\frac{j2\pi(pD+d)(\tau_{l_1}-\tau_{l_2}+\tau_{l_3}-\tau_{l_4})}{N_F}\right) \\ &\quad\times\sum_{r=0}^{N_{fn}-1}\exp\left(-\frac{j2\pi(\tau_{l_1}-\tau_{l_2}+\tau_{l_3}-\tau_{l_4})r}{N_{fn}}\right) \\ &= \frac{P_x^2P^2N_{fn}}{N_F^2}\sum_{d=0}^{D-2}\left(2\sum_{l_1=0}^{L-1}\sum_{l_2=0}^{L-1}|h_{l_1}|^2|h_{l_2}|^2 - \sum_{l=0}^{L-1}|h_l|^4\right) \\ &\le \frac{2P_x^2P^2(D-1)N_{fn}\kappa^2}{N_F^2} \end{aligned} \tag{C5}$$

mean zero and variance $((2P_x^2P^2(D-1)N_{fn}\kappa^2)/N_F^2) + ((2P_xP\sigma_n^2(D-1)N_{fn}\kappa)/N_F)$.

When $p \neq p_n$, we have

$$\chi_{p,q} = \sqrt{\frac{P_xP}{N_F}} \sum_{d=0}^{D-2} \sum_{r=0}^{N_{fn}-1} N\left(rN_{fs} + pD + d'\right) \times H^*\left(rN_{fs} + pD + d'\right) \psi_{p,q}^*\left(r(D-1) + d\right). \quad \text{(C6)}$$

Thus, we have $E\{\chi_{p,q}\} = 0$ and $\mathrm{Var}\{\chi_{p,q}\} = (2P_xP\sigma_n^2(D-1)N_{fn}\kappa)/N_F$ from (C3) for $p \neq p_n$.

ACKNOWLEDGMENT

The authors would like to thank the anonymous reviewers for their helpful and constructive comments and suggestions.

REFERENCES

[1] *High-Speed Physical Layer in the 5 GHz Band*, 1999. IEEE 802.11a.
[2] *Broadband Radio Access Networks (BRAN) HIPERLAN Type 2: Physical (PHY) Layer*, Apr. 2000. ETSI BRAN TS 101 475.
[3] *Radio Broadcasting Systems: Digital Audio Broadcasting (DAB) to Mobile, Portable and Fixed Receivers*, Sep. 2000. ETSI EN 300 401.
[4] *An Air Interface for Fixed Broadband Wireless Access Systems Part A: Systems Between 2 and 11 GHz*, Jul. 2001. IEEE 802.16ab-01/01r1.
[5] R. V. Nee and R. Prasad, *OFDM Wireless Multimedia Communications*. Norwood, MA: Artech House, 2000.
[6] *Physical Layer Procedures (FDD)*, Mar. 2000. 3GPP TS 25.125.
[7] M. Tanno, H. Atarashi, K. Higuchi, and M. Sawahashi, "Three-step cell search algorithm employing synchronization and common pilot channels for OFCDM broadband wireless access," *IEICE Trans. Commun.*, vol. E86-B, pp. 325–334, Jan. 2003.
[8] M. Fujii, "Cell search scheme embedded with carrier frequency synchronization in broadband OFDM-CDM systems," in *Proc. IEEE Globecom Conf.*, Taipei, Taiwan, R.O.C., Nov. 2001, vol. 1, pp. 17–21.
[9] K. S. Kim, K. H. Chang, S. W. Kim, and Y. S. Cho, "A preamble-based cell searching technique for OFDM cellular systems," in *Proc. IEEE VTC*, Orlando, FL, Oct. 2003, pp. 2471–2475.
[10] *Air Interface for Fixed and Mobile Broadband Wireless Access Systems: Amendment for Physical and Medium Access Control Layers for Combined Fixed and Mobile Operation in Licensed Bands*, Sep. 2004. IEEE 802.16e/D5.
[11] J. Terry and J. Heiskala, *OFDM Wireless LANs: A Theoretical and Practical Guide*. Indianapolis, IN: Sams, 2002.
[12] J.-J. Van De Beek, M. Sandell, and P. O. Börjesson, "ML estimation of time and frequency offset in OFDM systems," *IEEE Trans. Signal Process.*, vol. 45, no. 7, pp. 1800–1805, Jul. 1997.
[13] N. Lashkarian and S. Kiaei, "Globally optimum ML estimation of timing and frequency offset in OFDM systems," in *Proc. IEEE ICC*, New Orleans, LA, Jun. 2000, vol. 2, pp. 1044–1048.
[14] T. M. Schmidl and D. C. Cox, "Low-overhead, low-complexity [burst] synchronization for OFDM," in *Proc. IEEE Int. Conf. Converging Technol. Tomorrow's Appl.*, Jun. 1996, vol. 3, pp. 1301–1306.
[15] T. M. Schmidl and D. C. Cox, "Robust frequency and timing synchronization for OFDM," *IEEE Trans. Commun.*, vol. 45, no. 12, pp. 1613–1621, Dec. 1997.
[16] B. Park, H. Cheon, C. Kang, and D. Hong, "A novel timing estimation method for OFDM systems," *IEEE Commun. Lett.*, vol. 7, no. 5, pp. 239–241, May 2003.
[17] F. Tufvesson, O. Edfors, and M. Faulkner, "Time and frequency synchronization for OFDM using PN-sequence preambles," in *Proc. IEEE VTC*, Amsterdam, The Netherlands, Sep. 1999, vol. 4, pp. 2203–2207.
[18] A. Fort, J.-W. Weijers, V. Derudder, W. Eberle, and A. Bourdoux, "A performance and complexity comparison of auto-correlation and cross-correlation for OFDM burst synchronization," in *Proc. IEEE ICASSP*, Apr. 2003, vol. 2, pp. 341–344.
[19] P. H. Moose, "A technique for orthogonal frequency division multiplexing frequency offset correction," *IEEE Trans. Commun.*, vol. 42, no. 10, pp. 2908–2914, Oct. 1994.
[20] A. Papoulis and S. U. Pillai, *Probability, Random Variables, and Stochastic Processes*, 4th ed. New York: McGraw-Hill, 2002.
[21] J.-J. Van De Beek, O. Edfors, M. Sandell, S. K. Wilson, and P. O. Börjesson, "On channel estimation in OFDM systems," in *Proc. IEEE VTC*, Chicago, IL, Jul. 1995, vol. 2, pp. 815–819.
[22] J. G. Proakis, *Digital Communication*, 4th ed. New York: McGraw-Hill, 2000.
[23] S. J. Mason, "Feedback theory: Some properties of signal-flow graphs," *Proc. IRE*, vol. 41, no. 9, pp. 1144–1156, Sep. 1953.
[24] E. A. Sourour and S. C. Gupta, "Direct-sequence spread-spectrum parallel acquisition in a fading mobile channel," *IEEE Trans. Commun.*, vol. 38, no. 7, pp. 992–998, Jul. 1990.
[25] A. Annamalai and V. K. Bhargava, "Performance of selection diversity for DS/CDMA communications over Rayleigh fading channels," *Electron. Lett.*, vol. 32, no. 21, pp. 1966–1968, Oct. 1996.

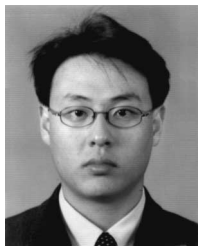

Kwang Soon Kim (S'94–M'99–SM'04) was born in Seoul, Korea, on September 20, 1972. He received the B.S. (*summa cum laude*), M.S.E., and Ph.D. degrees in electrical engineering from the Korea Advanced Institute of Science and Technology, Daejeon, Korea, in 1994, 1996, and 1999, respectively.

He was a recipient of the Postdoctoral Fellowship from the Korea Science and Engineering Foundation in 1999. From March 1999 to March 2000, he was with the Department of Electrical and Computer Engineering, University of California at San Diego, La Jolla, as a Postdoctoral Researcher. From April 2000 to February 2004, he was with the Mobile Telecommunication Research Laboratory, Electronics and Telecommunication Research Institute (ETRI), Daejeon, as a Senior Member of the Research Staff. Since March 2004, he has been with the Department of Electrical and Electronic Engineering, Yonsei University, Seoul, as an Assistant Professor. His research interests include detection and estimation theory, channel coding and iterative decoding, iterative receivers, adaptive modulation and coding, and wireless code-division multiple-access/orthogonal-frequency-division-multiplexing systems.

He received the Outstanding Researcher Award from ETRI in 2002.

Sung Woong Kim (S'03) received the B.S. and M.S. degrees in electronics engineering from Chung-Ang University, Seoul, Korea, in 2002 and 2004, respectively.

Since 2004, he has been with the Samsung Electronics Company, Ltd., Suwon, Korea, as a Development Engineer.

Yong Soo Cho (S'89–M'91–SM'07) received the B.S. degree in electronics engineering from Chung-Ang University, Seoul, Korea, the M.S. degree in electronics engineering from Yonsei University, Seoul, and the Ph.D. degree in electrical and computer engineering from the University of Texas at Austin in 1984, 1987, and 1991, respectively.

In 1984, he was a Research Engineer with the Goldstar Electrical Company, Osan, Korea. In 1992, he was with Chung-Ang University, where he is currently a Professor with the School of Electrical and Electronic Engineering. His research interests are in the area of wireless communication, particularly in multiple-input multiple-output orthogonal-frequency-division multiplexing.

Jae Young Ahn (M'06) received the B.Sc., M.Sc., and Ph.D. degrees from Yonsei University, Seoul, Korea, in 1983, 1985, and 1989, respectively.

Since 1989, he has been with the Electronics and Telecommunications Research Institute, Daejeon, Korea. From 1989 to 2002, he was involved in the development of satellite communications systems and wireless LAN technologies. Since 2003, he has been leading the development of radio transmission technologies for mobile communications. His current research interests include advanced radio transmission schemes and medium access control protocols for future wireless and mobile communications.